primary antibodies specific for Foxp3 (eBioscience, San Diego) overnight, followed by the additional incubation with Alexa Fluor 633 conjugated secondary antibodies (Molecular Probes, Eugene, OR, USA) for 30 min at room temperature. Sections were examined under Fluoview FV1000 laser scanning confocal microscopy (Olympus, Tokyo, Japan). The numbers of $Foxp3^+$ cells were counted in high power fields; five randomly chosen fields were evaluated.

Analysis of cytokine mRNA expression in mouse ears

At 6 h after the final challenge, the left ear skin was sampled. The specimen was homogenized and mRNA was extracted using Isogen (Nippon Gene, Tokyo, Japan) according to the manufacture's instruction; 1 ml of homogenate was vigorously mixed with 200 µl of chloroform, and then centrifuged at 15,000 rpm for 15 min at 4°C. Aqueous phase was separated and mixed with 0.5 ml of 2-propanol (Nacalai Tesque, Kyoto, Japan) to precipitate RNA. After centrifugation, the precipitate was washed with 1 ml of 75% ethanol (Nacalai Tesque) and dried up. RNA was suspended in 50 µl of RNase-free water, the concentration was calculated based on the absorbance at 260 nm, and the quality was confirmed by electrophoresis. cDNA was synthesized from 10 µg of mRNA using archive kit (ABI, Foster City, CA, USA) according to the manufacturer's protocol.

Cytokine mRNA expression in skin

Real time quantitative reverse transcription-polymerase chain reaction (RT-PCR) was performed to measure transcriptional activity in the skin lesions. A 25-µl reaction mixture containing 1 µg total of cDNA, 900 nmol of each primer, and 250 nmol of TaqMan probe were mixed with 12.5 µl of TaqMan Master Mix (ABI, Foster City, CA, USA). The following primers and probes were used for the PCR reactions: mouse IL-4; forward: 5′-ACAGGAGAA GGGACGCCAT-3′, reverse: 5′-GAAGCCCTACAGAC GAGCTCA-3′, probe: 5′-TCCTCACAGCAACGAAGAA CACCACA-3′-TAMRA, IFN-γ; forward: 5′-TCAAGTG GCATAGATGTGGAAGAA-3′, reverse: 5′-TGGCTCT GCAGGATTTTCATG-3′, probe: 5′-TCACCATCCTTTT GCCAGTTCCTCCAG-3′-TAMRA, IL-10; forward: 5′-G GTTGCCAAGCCTTATCGGA-3′, reverse: 5′-ACCTGCT CCACTGCCTTGCT, probe: 5′-TGAGGCGCTGTCGTC ATCGATTTCTCCC-3′-TAMRA, TGF-β; forward: 5′-TG ACGTCACTGGAGTTGTACGG-3′, reverse: 5′-GGTTC ATGTCATGGATGGTGC-3′, probe: 5′-TTCAGCGCTC ACTGCTCTTGTGACAG-3′-TAMRA, β-actin; forward: 5′-AGAGGGAAATCGTGCGTGAC-3′, reverse: 5′-CAA TAGTGATGACCTGGCCGT-3′, probe: 5′-CACTGCCG CATCCTCTTCCTCCC-3′-TAMRA [25]. PCR was performed under the following conditions: 95°C for 10 min, then 40 cycles of 95°C for 15 s, 60°C for 1 min were carried out. Fluorescence data were collected during each annealing-extension step and analyzed by using ABI Prism SDS software version 1.9.1. All samples were normalized for to the β-actin mRNA content.

Measurement of serum IgE

Blood was collected under anesthesia 6 h after the last challenge. Serum IgE levels were determined by a sandwich enzyme-linked immunosorbent assay (BD PharMingen, CA, USA) according to the manufacturer's instructions. Optical density of each well was determined by using a microplate reader (Multiscan JX) (Thermo Electron, Yokohama, Japan). Standard curve was prepared using mouse anti-TNP IgE standard (BD PharMingen, CA, USA) diluted with PBS containing 10% FCS.

Statistical analysis

Differences in ear swelling and serum IgE levels were analyzed by the Kruskal–Wallis test. $P < 0.05$ was taken as significant.

Results

Effect of Ag85B on skin inflammation

We first examined whether Ag85B could modulate ear-swelling reaction in a mouse model of OX-induced AD like skin lesions. Repeated applications of OX cause Th2-mediated immediate type response. Ear swelling was measured with thickness gauge calipers before and 30 min after OX challenge on the pinna of the ear on day 32. In both prophylactic and therapeutic models, the administration of Ag85B significantly suppressed swelling compared to placebo-treated controls (Fig. 2a). The OX-challenged placebo-treated mice showed severe skin inflammation, however administration of Ag85B DNA reduced atopic inflammatory reactions (Fig. 2b).

Histological analysis

Histological examination in OX-challenged mice showed epidermal hyperplasia and strong intraepidermal and intradermal inflammatory cell infiltration including mononuclear cells, neutrophils, and granular cells (Fig. 3a). Both prophylactic and therapeutic administration of Ag85B DNA clearly reduced inflammatory cell infiltration and epidermal thickness. Skin sections stained with truidine blue showed decreased mast cell infiltration in Ag85B-treated mice (Fig. 3b).

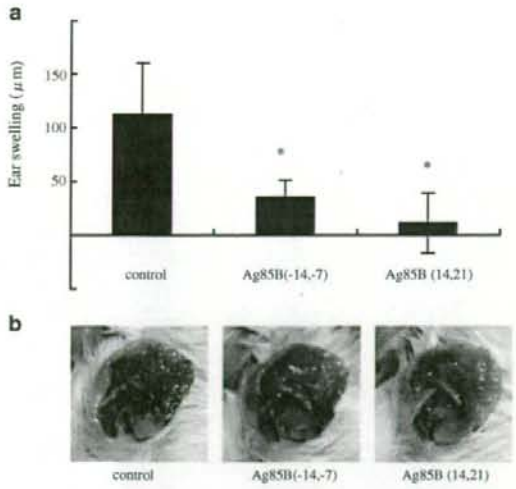

Fig. 2 **a** OX-induced ear swelling. The ear swelling response was expressed as the difference between ear thickness before and 30 min after each application on day 32. The columns and error bars represent mean ± SEM. $^*P < 0.05$. Swelling was suppressed significantly in Ag85B-treated mice compared with those in placebo-treated mice. **b** Clinical features of ear skin on day 35. The OX-challenged mice showed severe skin eruption, however administration of the Ag85B DNA in both prophylactic and therapeutic models clearly reduced atopic inflammatory reactions in OX-sensitized mice

Ag85B treatment shifted the Th1/Th2 balance toward Th1

IFN-γ and IL-12 shift the Th1/Th2 balance toward Th1 condition; while IL-4 and IL-5 are key cytokines in Th2 response [24, 29]. To clarify the type of immune response in skin lesions after treatment with Ag85B, we analyzed the mRNA expression levels of IL-4 and IFN-γ by real time quantitative RT-PCR. The results were normalized to the β-actin mRNA content. As shown in Fig. 4, the expression of IL-4 mRNA was reduced in Ag85B-treated mice in both prophylactic and therapeutic models. On the contrary, the expression of IFN-γ was enhanced in Ag85B-treated mice. These results suggest that the application of Ag85B shifts the immune response toward Th1-predominace.

Total serum IgE levels

Atopic dermatitis is characterized by elevated IgE levels. Repeated applications of OX cause a gradual elevation of antigen-specific IgE level. We analyzed the degrees of IgE levels in sera collected from experimental mice. Administration of Ag85B significantly reduced the serum levels of IgE (Fig. 5).

Ag85B treatment induces regulatory T cells

TGF-β and IL-10 are important regulatory cytokines produced by Treg [11]. To investigate the mechanisms of the therapeutic effectiveness of Ag85B, we examined the mRNA levels of TGF-β and IL-10. As shown in Fig. 6a, TGF-β and IL-10 were significantly increased in Ag85B-treated mice in both prophylactic and therapeutic models. And then, we next looked at the induction of Treg in the inflamed skin. Naturally occurring $CD4^+CD25^+$ Treg are characterized by the expression of Foxp3 [10, 27]. Skin sections were stained with anti-Foxp3 mAb, and examined with a fluorescent microscope. As shown in Fig. 6b, $Foxp3^+$ cells were increased in the Ag85B-treated mice.

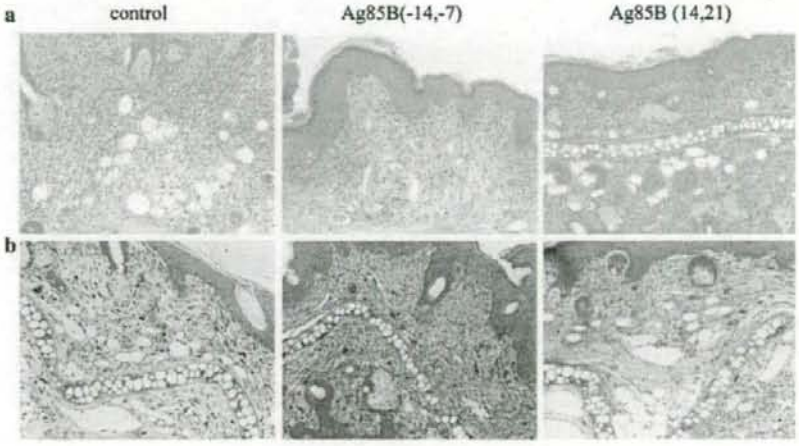

Fig. 3 Histopathological features of skin lesions. Skin was taken on day 35, paraffin embedded sections were stained with **a** hematoxylin and eosin or **b** truidine blue. OX-challenged mice showed epidermal hyperplasia along with strong intradermal inflammatory cell infiltration; whereas Ag85B DNA significantly reduced the inflammatory changes

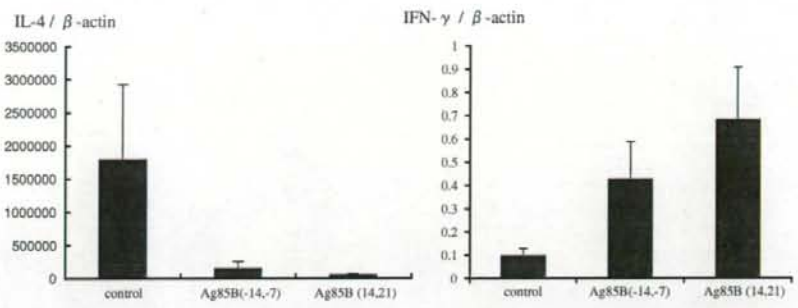

Fig. 4 mRNA expression in the ear on day 35. In order to clarify the expression of cytokine mRNA, quantitative PCR was performed by using specific primers and probes for IL-4 and IFN-γ. The expression of IL-4 mRNA was reduced in Ag85B-treated mice compared with placebo-treated mice. On the other hand, mRNA expression of IFN-γ was significantly increased in Ag85B mice

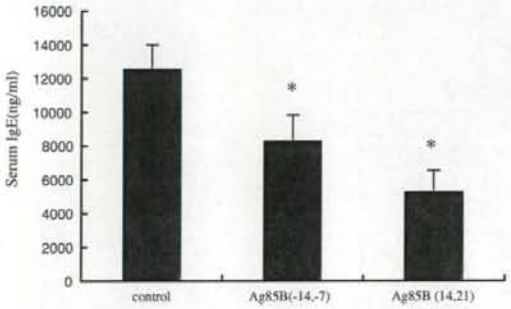

Fig. 5 Serum IgE concentrations. Serum IgE levels were measured on day 35 in control, Ag85B DNA IP (−14, −7), or Ag85B DNA IP (14, 21) mice. The columns and error bars represent mean ± SEM. $^*P < 0.05$. Administration of Ag85B reduced IgE level

Discussion

Human immune system responds to exogenous microorganisms for self-protection. These responses lead to Th1 and/ or Th2 type cytokine secretion depending on the nature of stimuli. AD is a chronic dermatitis characterized by a Th2-type immune responses that causes elevation of IgE. On the other hand, some bacterial infections including *Mycobacterium* species elicits strong Th1-type responses. Inducers of Th1 type immune response may be used as immuno-modulator having therapeutic effects against allergic disease elicited by Th2-type immune responses. Mycobacteria may affect atopic disorders by correction of the immune response from Th2 to Th1. Erb et al. reported that *M. bovis* (BCG) suppresses airway eosinophilia and associated local IL-5 production by inducing Th1-mediated response [9]. Furthermore, recent studies suggested that mycobacteria induce not only Th cells providing Th1 type immune responses but also Treg cells. In an animal model of allergy, the immunomodulatory effects of *M. vaccae* was found to be mediated by allergen-specific regulatory T lymphocytes [37], and oral administration of *M. vaccae* inhibited pulmonary allergic inflammation by induction of IL-10 [14].

Alive BCG vaccination has been used for prevention of tuberculosis. The use of *Mycobacterium* for immunomodulation requires repeated exposures to the immune system. However, repeated alive BCG vaccination is contraindicated. For human therapeutic application, it needs intradermal or intramuscular injection for vaccination. Unfortunately, cutaneous vaccination with *Mycobacterium* species commonly produces granulomatous formation leading to recalcitrant ulcers. We need to develop Th1 type immunomodulating system that induces no granulomatous reaction, if species of mycobacteria are tried to use for human. The Ag85B protein is a main component of the cell wall of mycobacteria such as *M. tuberculosis and M. kansasii* [4]; this Ag85B is known as a strong Th1 inducer in vitro [17, 18]. Experiments using plasmid DNA encoding Ag85B has been previously reported. This Ag85B is able to protect against *M. tuberculosis* even in Balb/c mice [33]. Intraperitoneal administration of Ag85B DNA inhibits granulomatous changes or adhesive reaction of intraperitoneal organs in mice (data not shown). As a preliminary study, Ag85B DNA was intradermally injected in the skin of mice skin. No ulcerative changes were observed in vaccinated areas of the skin (data not shown).

In our present study, we evaluated the efficacy of DNA encoding Ag85B for inducing Th1- and Treg-type immune response in OX-induced acute phase dermatitis. Repeated applications of OX in mice ears caused Th2-type dominant dermatitis, which mimic most of the characteristic features of AD [16, 19, 20, 32]. We first investigated whether the application of Ag85B corrects the immune response from a type Th2 one to a type Th1 response. Our results showed that Ag85B successfully ameliorates Th2-cytokine dominant immediate type reaction in the skin lesions in both prophylactic and therapeutic models of the disease. In Ag85B-treated AD skin lesion, the ear swelling was significantly reduced compared to placebo-treated animals. Administration of Ag85B DNA suppressed histological abnormalities caused by atopic inflammations such as inflammatory cell infiltration, epidermal hyperplasia, and severe edema. The presence of mast cells in the skin lesion is closely associated with Th2-type dermatitis; the number of mast cells was

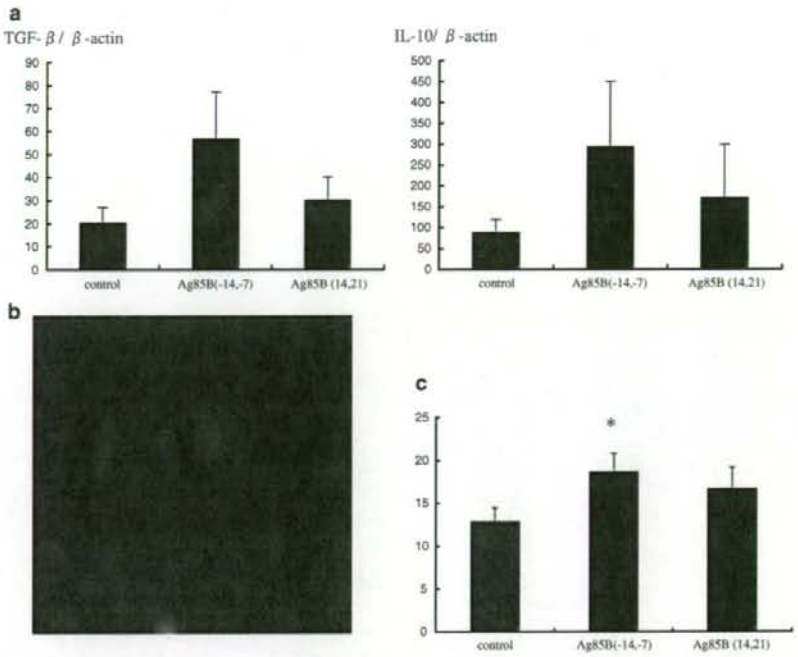

Fig. 6 **a** mRNA expression in the ear on day 35. Quantitative PCR was performed by using specific primers and probes for IL-10 and TGF-β. Both TGF-β and IL-10 were increased in the Ag85B-treated mice. **b** Foxp3$^+$ cells were clearly observed with confocal microscopy. **c** The number of Foxp3$^+$ cells per HPF was counted in five nonconsecutive fields, and Foxp3$^+$ cells were found to be increased in Ag85B-treated mice

increased in OX-treated control animals as expected; however, the number of mast cells was decreased in Ag85B-treated mice compared with controls. Enhancement of the expression of IFN-γ mRNA was significant in Ag85B-treated AD mice compared with placebo-treated animals. The expression of IL-4 mRNA were suppressed in Ag85B-treated mice compared to placebo-treated controls (Fig. 4). In addition, serum IgE levels were significantly suppressed in Ag85B treated mice compared with placebo-treated mice. These finding demonstrates that administration of Ag85B DNA significantly inhibited the development of Th2-cytokine dominant atopic inflammation by inducing Th1-type immune response.

We also examined the potential of Ag85B to induce Treg cell responses. TGF-β and IL-10 have been described as critical regulatory cytokines produced by Treg [11]. Heat-killed *M. vaccae* induces regulatory T cells that secrete IL-10 and TGF-β [37]. *M. vaccae* also induces a population of CD11$^+$ cells characterized by an increased expression of regulatory cytokines including IL-10 and TGF-β[1]. Treg cells are developed mainly in the presence of IL-10 and TGF-β [13]. More recently, Inoue and Aramaki reported that topical application of CpG-Oligodeoxynucleotides induces Foxp3$^+$ Treg in skin lesions of AD model mice in association with elevation of TGF-β[15]. Depletion of CD4$^+$CD25$^+$Treg from the peripheral blood of healthy individuals enhances proliferation of Th2 in response to various allergens [6, 23]. The mechanisms of the suppressive activity of Treg depend on cell-to-cell contact, and there is evidence for the involvement of IL-10 and TGF-β[2, 3, 26]. In this study, we have shown elevated expression of TGF-β and IL-10 in Ag85B-treated mice (Fig. 6a), and Foxp3$^+$ Treg was increased in the Ag85B-treated skin (Fig. 6b). We assume that the therapeutics capability of Ag85B is related to the induction of Foxp3$^+$Treg and Th1-type immune response.

In brief, in this study we have shown the usefulness of plasmid DNA of Ag85B for the amelioration of Th1/Th2 imbalance and for the generation of Treg cells. The observations suggest that Ag85B may be useful for the prevention and treatment of atopic disorders.

Acknowledgments This work was supported in part by Health Science Research Grants from the Ministry of Health, Labor and Welfare of Japan and the Ministry of Education, Culture, Sports, Science and Technology of Japan, Grants-in-Aid for Scientific Research and Grants-in-Aid for Core Research Evolutional Science and Technology.

Conflicts of interest statement None.

References

1. Adams VC, Hunt JR, Martinelli R, Palmer R, Rook GA, Brunet LR (2004) *Mycobacterium vaccae* induces a population of pulmonary CD11c+ cells with regulatory potential in allergic mice. Eur J Immunol 34:631–638

2. Akdis M, Verhagen J, Taylor A, Karamloo F, Karagiannidis C, Crameri R, Thunberg S, Deniz G, Valenta R, Fiebig H, Kegel C, Disch R, Schmidt-Weber CB, Blaser K, Akdis CA (2004) Immune responses in healthy and allergic individuals are characterized by a fine balance between allergen-specific T regulatory 1 and T helper 2 cells. J Exp Med 199:1567–1575
3. Asseman C, Mauze S, Leach MW, Coffman RL, Powrie F (1999) An essential role for interleukin 10 in the function of regulatory T cells that inhibit intestinal inflammation. J Exp Med 190:995–1004
4. Belisle JT, Vissa VD, Sievert T, Takayama K, Brennan PJ, Besra GS (1997) Role of the major antigen of *Mycobacterium tuberculosis* in cell wall biogenesis. Science 276:1420–1422
5. Burney PG, Chinn S, Rona RJ (1990) Has the prevalence of asthma increased in children? Evidence from the national study of health and growth 1973–86. BMJ 300:1306–1310
6. Cavani A, Nasorri F, Ottaviani C, Sebastiani S, De Pita O, Girolomoni G (2003) Human CD25+ regulatory T cells maintain immune tolerance to nickel in healthy, nonallergic individuals. J Immunol 171:5760–5768
7. Cookson WO, Moffatt MF (1997) Asthma: an epidemic in the absence of infection? Science 275:41–42
8. Del Prete G (1992) Human Th1 and Th2 lymphocytes: their role in the pathophysiology of atopy. Allergy 47:450–455
9. Erb KJ, Holloway JW, Sobeck A, Moll H, Le Gros G (1998) Infection of mice with *Mycobacterium bovis*-Bacillus Calmette-Guerin (BCG) suppresses allergen-induced airway eosinophilia. J Exp Med 187:561–569
10. Fontenot JD, Gavin MA, Rudensky AY (2003) Foxp3 programs the development and function of CD4+CD25+ regulatory T cells. Nat Immunol 4:330–336
11. Groux H, O'Garra A, Bigler M, Rouleau M, Antonenko S, de Vries JE, Roncarolo MG (1997) A CD4+ T-cell subset inhibits antigen-specific T-cell responses and prevents colitis. Nature 389:737–742
12. Herz U, Gerhold K, Gruber C, Braun A, Wahn U, Renz H, Paul K (1998) BCG infection suppresses allergic sensitization and development of increased airway reactivity in an animal model. J Allergy Clin Immunol 102:867–874
13. Horwitz DA, Zheng SG, Gray JD (2003) The role of the combination of IL-2 and TGF-beta or IL-10 in the generation and function of CD4+ CD25+ and CD8+ regulatory T cell subsets. J Leukoc Biol 74:471–478
14. Hunt JR, Martinelli R, Adams VC, Rook GA, Brunet LR (2005) Intragastric administration of *Mycobacterium vaccae* inhibits severe pulmonary allergic inflammation in a mouse model. Clin Exp Allergy 35:685–690
15. Inoue J, Aramaki Y (2007) Suppression of skin lesions by transdermal application of CpG-oligodeoxynucleotides in NC/Nga mice, a model of human atopic dermatitis. J Immunol 178:584–591
16. Inoue Y, Isobe M, Shiohara T, Goto Y, Hayashi H (2002) Protective and curative effects of topically applied CX-659S, a novel diaminouracil derivative, on chronic picryl chloride-induced contact hypersensitivity responses. Br J Dermatol 147:675–682
17. Kariyone A, Higuchi K, Yamamoto S, Nagasaka-Kametaka A, Harada M, Takahashi A, Harada N, Ogasawara K, Takatsu K (1999) Identification of amino acid residues of the T-cell epitope of *Mycobacterium tuberculosis* alpha antigen critical for Vbeta11(+) Th1 cells. Infect Immun 67:4312–4319
18. Kariyone A, Tamura T, Kano H, Iwakura Y, Takeda K, Akira S, Takatsu K (2003) Immunogenicity of Peptide-25 of Ag85B in Th1 development: role of IFN-gamma. Int Immunol 15:1183–1194
19. Kitagaki H, Fujisawa S, Watanabe K, Hayakawa K, Shiohara T (1995) Immediate-type hypersensitivity response followed by a late reaction is induced by repeated epicutaneous application of contact sensitizing agents in mice. J Invest Dermatol 105:749–755
20. Kitagaki H, Ono N, Hayakawa K, Kitazawa T, Watanabe K, Shiohara T (1997) Repeated elicitation of contact hypersensitivity induces a shift in cutaneous cytokine milieu from a T helper cell type 1 to a T helper cell type 2 profile. J Immunol 159:2484–2491
21. Kitagaki H, Kimishima M, Teraki Y, Hayakawa J, Hayakawa K, Fujisawa S, Shiohara T (1999) Distinct in vivo and in vitro cytokine profiles of draining lymph node cells in acute and chronic phases of contact hypersensitivity: importance of a type 2 cytokine-rich cutaneous milieu for the development of an early-type response in the chronic phase. J Immunol 163:1265–1273
22. Kuromatsu I, Matsuo K, Takamura S, Kim G, Takebe Y, Kawamura J, Yasutomi Y (2001) Induction of effective antitumor immune responses in a mouse bladder tumor model by using DNA of an alpha antigen from mycobacteria. Cancer Gene Ther 8:483–490
23. Ling EM, Smith T, Nguyen XD, Pridgeon C, Dallman M, Arbery J, Carr VA, Robinson DS (2004) Relation of CD4+CD25+ regulatory T-cell suppression of allergen-driven T-cell activation to atopic status and expression of allergic disease. Lancet 363:608–615
24. McKnight AJ, Zimmer GJ, Fogelman I, Wolf SF, Abbas AK (1994) Effects of IL-12 on helper T cell-dependent immune responses in vivo. J Immunol 152:2172–2179
25. Overbergh L, Valckx D, Waer M, Mathieu C (1999) Quantification of murine cytokine mRNAs using real time quantitative reverse transcriptase PCR. Cytokine 11:305–312
26. Powrie F, Carlino J, Leach MW, Mauze S, Coffman RL (1996) A critical role for transforming growth factor-beta but not interleukin 4 in the suppression of T helper type 1-mediated colitis by CD45RB(low) CD4+ T cells. J Exp Med 183:2669–2674
27. Sakaguchi S, Sakaguchi N, Shimizu J, Yamazaki S, Sakihama T, Itoh M, Kuniyasu Y, Nomura T, Toda M, Takahashi T (2001) Immunologic tolerance maintained by CD25+ CD4+ regulatory T cells: their common role in controlling autoimmunity, tumor immunity, and transplantation tolerance. Immunol Rev 182:18–32
28. Shirakawa T, Enomoto T, Shimazu S, Hopkin JM (1997) The inverse association between tuberculin responses and atopic disorder. Science 275:77–79
29. Swain SL, Weinberg AD, English M, Huston G (1990) IL-4 directs the development of Th2-like helper effectors. J Immunol 145:3796–3806
30. Takamura S, Matsuo K, Takebe Y, Yasutomi Y (2005) Ag85B of mycobacteria elicits effective CTL responses through activation of robust Th1 immunity as a novel adjuvant in DNA vaccine. J Immunol 175:2541–2547
31. Takatsu K, Kariyone A (2003) The immunogenic peptide for Th1 development. Int Immunopharmacol 3:783–800
32. Tamura T, Matsubara M, Hasegawa K, Ohmori K, Karasawa A (2005) Olopatadine hydrochloride suppresses the rebound phenomenon after discontinuation of treatment with a topical steroid in mice with chronic contact hypersensitivity. Clin Exp Allergy 35:97–103
33. Teixeira FM, Teixeira HC, Ferreira AP, Rodrigues MF, Azevedo V, Macedo GC, Oliveira SC (2006) DNA vaccine using *Mycobacterium bovis* Ag85B antigen induces partial protection against experimental infection in BALB/c mice. Clin Vaccine Immunol 13:930–935
34. Ulmer JB, Montgomery DL, Tang A, Zhu L, Deck RR, DeWitt C, Denis O, Orme I, Content J, Huygen K (1998) DNA vaccines against tuberculosis. Novartis Found Symp 217:239–246 discussion 246–253
35. Yazdanbakhsh M, Kremsner PG, van Ree R (2002) Allergy, parasites, and the hygiene hypothesis. Science 296:490–494
36. Zhu D, Jiang S, Luo X (2005) Therapeutic effects of Ag85B and MPT64 DNA vaccines in a murine model of *Mycobacterium tuberculosis* infection. Vaccine 23:4619–4624
37. Zuany-Amorim C, Sawicka E, Manlius C, Le Moine A, Brunet LR, Kemeny DM, Bowen G, Rook G, Walker C (2002) Suppression of airway eosinophilia by killed *Mycobacterium vaccae*-induced allergen-specific regulatory T-cells. Nat Med 8:625–629

Prior Immunization with Severe Acute Respiratory Syndrome (SARS)-Associated Coronavirus (SARS-CoV) Nucleocapsid Protein Causes Severe Pneumonia in Mice Infected with SARS-CoV[1]

Fumihiko Yasui,* Chieko Kai,[‡] Masahiro Kitabatake,[2]* Shingo Inoue,[‖] Misako Yoneda,[‡] Shoji Yokochi,*[§] Ryoichi Kase,* Satoshi Sekiguchi,* Kouichi Morita,[‡] Tsunekazu Hishima,[¶] Hidenori Suzuki,[†] Katsuo Karamatsu,[#] Yasuhiro Yasutomi,[#] Hisatoshi Shida,[**] Minoru Kidokoro,[††] Kyosuke Mizuno,[‡‡] Kouji Matsushima,[§] and Michinori Kohara[3]*

The details of the mechanism by which severe acute respiratory syndrome-associated coronavirus (SARS-CoV) causes severe pneumonia are unclear. We investigated the immune responses and pathologies of SARS-CoV-infected BALB/c mice that were immunized intradermally with recombinant vaccinia virus (VV) that expressed either the SARS-CoV spike (S) protein (LC16m8rVV-S) or simultaneously all the structural proteins, including the nucleocapsid (N), membrane (M), envelope (E), and S proteins (LC16m8rVV-NMES) 7–8 wk before intranasal SARS-CoV infection. The LC16m8rVV-NMES-immunized group exhibited as severe pneumonia as the control groups, although LC16m8rVV-NMES significantly decreased the pulmonary SARS-CoV titer to the same extent as LC16m8rVV-S. To identify the cause of the exacerbated pneumonia, BALB/c mice were immunized with recombinant VV that expressed the individual structural proteins of SARS-CoV (LC16mOrVV-N, -M, -E, -S) with or without LC16mOrVV-S (i.e., LC16mOrVV-N, LC16mOrVV-M, LC16mOrVV-E, or LC16mOrVV-S alone or LC16mOrVV-N + LC16mOrVV-S, LC16mOrVV-M + LC16mOrVV-S, or LC16mOrVV-E + LC16mOrVV-S), and infected with SARS-CoV more than 4 wk later. Both LC16mOrVV-N-immunized mice and LC16mOrVV-N + LC16mOrVV-S-immunized mice exhibited severe pneumonia. Furthermore, LC16mOrVV-N-immunized mice upon infection exhibited significant up-regulation of both Th1 (IFN-γ, IL-2) and Th2 (IL-4, IL-5) cytokines and down-regulation of anti-inflammatory cytokines (IL-10, TGF-β), resulting in robust infiltration of neutrophils, eosinophils, and lymphocytes into the lung, as well as thickening of the alveolar epithelium. These results suggest that an excessive host immune response against the nucleocapsid protein of SARS-CoV is involved in severe pneumonia caused by SARS-CoV infection. These findings increase our understanding of the pathogenesis of SARS. *The Journal of Immunology,* **2008, 181: 6337–6348.**

From November 2002 to July 2003, an outbreak of severe acute respiratory syndrome (SARS),[4] which originated in China, spread worldwide, resulting in 8098 cases with 774 deaths (http://www.who.int/csr/sars/country/en/index.html). Patients with SARS usually develop high fever followed by severe clinical symptoms, which include acute respiratory distress syndrome with diffuse alveolar damage, and ultimately death. A novel type of coronavirus (CoV), termed SARS-associated CoV (SARS-CoV), was identified as the etiologic agent of SARS (1–3). The genome of SARS-CoV is a single strand of positive-sense RNA of ~30 kb in length with 14 putative open reading frames, which encode nonstructural replicase polyproteins and several structural proteins, including spike (S), envelope (E), membrane (M), and nucleocapsid (N) proteins (4). The S protein of SARS-CoV, like the S proteins of other CoVs, plays an important role in the first step of viral infection by binding to a host cell receptor. Angiotensin-converting enzyme 2 was identified as the host receptor for SARS-CoV (5). Angiotensin-converting enzyme 2 is abundantly expressed in the epithelia of the lung and small intestine and may mediate SARS-CoV entry in humans (6). Although intensive investigations rapidly unraveled the sequence of the SARS-CoV genome and its receptor in humans, the precise molecular mechanism underlying the development of SARS is not fully understood.

The possible roles of host anti-SARS-CoV immune responses have been suggested in severe clinical cases. The uncontrolled release of immune mediators, called a "cytokine storm," has been

*Department of Microbiology and Cell Biology, [†]Laboratory of Electron Microscopy, The Tokyo Metropolitan Institute of Medical Science, [‡]Laboratory Animal Research Center, The Institute of Medical Science, [§]Department of Molecular Preventive Medicine, School of Medicine, The University of Tokyo, and [¶]Department of Pathology, Tokyo Metropolitan Komagome Hospital, Tokyo, Japan; [‖]Department of Virology, Institute of Tropical Medicine, Nagasaki University, Nagasaki, Japan; [#]Laboratory of Immunoregulation and Vaccine Research, Tsukuba Primate Research Center, National Institute of Biomedical Innovation, Ibaraki, Japan; [**]Division of Molecular Virology, Institute for Genetic Medicine, Hokkaido University, Sapporo, Japan; [††]Third Department of Virology, National Institute of Infectious Diseases, Musashimurayama, Japan; and [‡‡]The Chemo-Sero-Therapeutic Research Institute, Kumamoto, Japan

Received for publication January 23, 2008. Accepted for publication August 23, 2008.

The costs of publication of this article were defrayed in part by the payment of page charges. This article must therefore be hereby marked *advertisement* in accordance with 18 U.S.C. Section 1734 solely to indicate this fact.

[1] This study was supported in part by a Grant for Research on Emerging and Re-emerging Infectious Diseases from the Ministry of Health, Labor and Welfare, Japan, by the 21st Century Centers of Excellence program on Global Strategies for Control of Tropical and Emerging Infectious Diseases at Nagasaki University, and by the Ministry of Education, Culture, Sports, Science and Technology of Japan. Strategic cooperation to control emerging and re-emerging infections is funded by the Special Co-ordination Fund for Promoting Science and Technology of the Ministry of Education, Culture, Sports, Science and Technology.

[2] Current address: Department of Immunology, Graduate School of Medicine, Kumamoto University, 1-1-1 Honjo, Kumamoto, 860-8556, Japan.

[3] Address correspondence and reprint requests to Dr. Michinori Kohara, Department of Microbiology and Cell Biology, The Tokyo Metropolitan Institute of Medical Science, 3-18-22 Honkomagome, Bunkyo-ku, Tokyo 113-8613, Japan. E-mail address: kohara-mc@igakuken.or.jp

[4] Abbreviations used in this paper: SARS, severe acute respiratory syndrome; CoV, coronavirus; VV, vaccinia virus; HA, hemagglutinin; MOI, multiplicity of infection; VLP, virus-like particle; $TCID_{50}$, tissue culture ID_{50}.

implicated in the pathogenesis of SARS. However, the cytokine profiles of SARS patient sera do not correlate with the severity of pneumonia because of their diversity. For example, Jones et al. (7) have reported a decreased number of IL-2-, IL-4-, IL-10-, and IL-12-producing cells in SARS-CoV-infected patients. In contrast, Wong et al. (8) have demonstrated increased production of IFN-γ, IL-1, IL-6, and IL-12 p70, but not of IL-2, IL-4, IL-10 or TNF-α, which is consistent with a Th1 response. The data from these adult patients with SARS show no clear trend toward either a Th1 or Th2 bias. These results might be related to patient anamnesis. Therefore, the development of animal models for SARS is needed to understand the pathogenesis of SARS. Non-human primates, mice, ferrets, and hamsters have been found to support the replication of SARS-CoV (9–14). However, an animal model that mimics the clinical symptoms and pathology observed in SARS patients has not been reported to date. Recently, Roberts et al. (15) reported that aged BALB/c mice (older than 12 mo) exhibited high and prolonged levels of viral replication, signs of clinical symptoms, and histopathologic changes in the lung. Aged BALB/c mice represent a conventional animal model that mimics the findings in elderly SARS patients, many of whom exhibit severe disease requiring intensive care and ventilation support, as well as increased mortality.

In the present study, we investigated the pulmonary immune responses and pathologies of intranasally SARS-CoV-infected BALB/c mice older than 6 mo of age that were previously immunized with SARS-CoV structural proteins using vaccinia virus (VV) vectors, by measuring various cytokine mRNAs and histopathologies of the lungs.

Materials and Methods

Cells and viruses

RK13 cells (CCL-37) from the American Type Culture Collection (ATCC) and Vero E6 cells (CRL-1586) from ATCC were cultured in MEM (Nissui Pharmaceutical) that contained 5% FCS. To generate recombinant VV LC16m8, which expresses the structural proteins of SARS-CoV, primary rabbit kidney cell cultures were prepared by overnight digestion with 100 PU/ml dispase (Sanko Jun-yaku) of kidneys extirpated from 7-day-old inbred JW rabbits (Kitayama Labs). The cells were grown in T175 flasks in lactalbumin medium with Hank's salts (LH) that contained 5% FCS, 100 U/ml penicillin, and 100 μg/ml streptomycin. When the cell confluency was ~50%, the culture medium was replaced with lactalbumin medium with Eagle's salts (LE) that contained 5% FCS, 100 U/ml penicillin, and 100 μg/ml streptomycin. SARS-CoV Vietnam/NB-04/2003 strain, which was isolated from the throat wash fluid of one patient (16), was provided by Dr. M. Quynh Le. VVs LC16m8 (m8) and LC16mO (mO) were provided by the Chemo-Sero-Therapeutic Research Institute (Kumamoto, Japan). All work using SARS-CoV was performed in BioSafety Level 3 facilities by personnel wearing powered air-purifying respirators (Shigematsu Works).

Generation of recombinant VV

To generate a pBR322-based plasmid vector (pBMSF) for homologous recombination into the hemagglutinin (HA) locus of m8, we cloned the HA gene, which contained the ATI/p7.5 synthetic hybrid promoter, from the pSFJ1–10 plasmid and inserted it into the pBM vector, which was reconstructed in our laboratory. Full-length cDNAs for the SARS-CoV nucleocapsid (N), membrane (M), and envelope (E) proteins were cloned from the Vietnam/NB-04/2003 strain of SARS-CoV by RT-PCR (16). Full-length SARS-CoV spike (S) protein gene was prepared from pSFJ1-10-SARS-S, which is described in our previous report (17). Next, the genes that encode the SARS-CoV structural proteins were ligated by inserting internal ribosomal entry site sequence of hepatitis C virus (genotypes 2a and 1b/2b) fused with the 2A sequence of foot and mouth disease virus and *Thosea asigna* virus or encephalomyocarditis virus by PCR (see Fig. 1*A*). The generated DNA fragment was digested with *Eco*RI and inserted downstream of the ATI/p7.5 hybrid promoter of pBR322-based plasmid vector pBMSF, thereby generating pBMSF-SARS-NMES. The pBMSF-SARS-NMES plasmid was linearized with *Pvu*I, and transfected into primary rabbit kidney cells that had been infected with m8 at a multiplicity of infection (MOI) of 10. After 36 h, the virus-cell mixture were harvested by scraping, and frozen at −80°C until use. The resulting HA-negative recombinant viruses were purified as previously described (17), and named m8rVV-NMES. Furthermore, recombinant mO that expressed the SARS-CoV N, M, or E protein with a six histidine tag at the C terminus was generated (mOrVV-NHis, mOrVV-MHis, and mOrVV-EHis), as was mO that expressed six histidine-tagged S protein (mOrVV-SHis), as previously described (17).

Western blot analysis

Vero E6 cells were infected with m8rVV-NMES at an MOI of 5. After 18 h, the cells were lysed with lysis buffer (10 mM Tris (pH 7.4), 150 mM NaCl, 1% SDS, 0.5% Nonidet P-40, protease inhibitor cocktail). The cell lysates (30 μg) were resolved by SDS-PAGE and transferred to a polyvinylidene difluoride membrane (Immobilon-P; Millipore). After blocking the membranes with 5% skim milk solution at room temperature for 1 h, the membrane was incubated with polyclonal Abs against the N, M, E, or S protein. Vero E6 cell lysates infected with mOrVV-NHis, mOrVV-MHis, mOrVV-EHis, or mOrVV-SHis was used as positive controls. We used the anti-S polyclonal Abs described in our previous study (17). Polyclonal Abs against N and E proteins were prepared from rabbit sera immunized with KLH-conjugated N peptide (residues aa 250–263) and E peptide (residues aa 61–73). Polyclonal Abs against the M protein were provided by Dr. Mizutani (National Institute of Infectious Diseases, Musashimurayama, Tokyo). We purified the IgG fractions of these antisera using the protein A Ampure PA kit (Amersham Biosciences). After washing with TBS that contained 0.1% Tween 20 (TBST), the membranes were reacted with HRP-conjugated $F(ab')_2$ of anti-rabbit IgG (GE Healthcare). Each specific protein band was visualized using the ECL system (GE Healthcare).

Indirect immunofluorescence analysis

Vero E6 cells were infected with m8rVV-NMES at an MOI of 5 at 30°C for 4 h. The cells were washed with PBS and fixed with cold acetone/methanol (1/1) mixture for 10 min. After blocking with TNB blocking buffer (NEN Life Science Products) at room temperature for 1 h, the fixed cells were incubated with polyclonal Abs against the N, M, or E protein or mAb against the S protein (designated as anti-S-His protein, clone no. 13B8), which was originally prepared in our laboratory, at 4°C overnight. After washing, the cells were incubated with Alexa Fluor 488-conjugated anti-rabbit IgG or mouse IgG Ab at room temperature for 1 h. Nuclei were stained with DAPI (4′,6-diamidino-2-phenylindole). Fluorescence images were acquired using a confocal microscope (LSM510 META; Carl Zeiss).

Confirmation of SARS-CoV-like particle formation

RK13 cells were cultured in 150-mm dishes, and then infected with m8rVV-NMES at an MOI of 5. After 48 h of incubation, the culture supernatants were collected and centrifuged to remove cell debris at 3000 rpm for 30 min at 4°C. The supernatants were concentrated ~100-fold using the Pellicon XL (cut off molecular weight 3×10^5; Millipore). The isolation of virus-like particles (VLP) was performed as previously described, with a slight modification (18). Briefly, the concentrated supernatant was placed on 60% (w/w) sucrose cushion and centrifuged at 4.0×10^4 rpm for 5 h. The opalescent band was collected and centrifuged in a 20–60% (w/w) sucrose gradient at 2.7×10^4 rpm for 4 h, and then divided into 20 fractions. The protein content of each fraction was determined with the DC protein assay kit (Bio-Rad). The 20 μl of each fraction were separated by SDS-PAGE (7.5%, 10%, or 15% polyacrylamide gel), and transferred onto a polyvinylidene difluoride membrane. The membrane was incubated with mAb against S protein (13B8), mAb against N protein (IMG-654; Imgenex) or polyclonal Abs against the M or E protein. After washing, the membranes were reacted and visualized as described. The VLPs in the concentrated culture supernatant were visualized using transmission electron microscopy. For immunogold staining, VLPs were loaded onto a collodion-coated electron microscopy grid for 5 min. After the removal of excess sample solution, polyclonal Ab against S protein was added onto the grid and incubated at room temperature for 1 h. The grids were washed six times with Sorensen's phosphate buffer at room temperature and incubated with 5-nm gold-conjugated anti-rabbit IgG for 1 h. After washing with Sorensen's phosphate buffer for 10 s, the samples were stained with 2% phosphotungstic acid for 1 min. After draining off the excess phosphotungstic acid, the samples were observed under the electron microscopy.

Immunization of rabbits with m8rVV-NMES

Groups of three New Zealand White rabbits (SLC) were immunized intradermally with 1×10^8 PFU/body of m8rVV-NMES or with 1×10^8 PFU/body of m8, at 0 and 6 wk. Sera were collected at the indicated time

points (see Fig. 2A), and used in ELISA analysis and in the in vitro neutralization assay described below. All animal experiments using rabbits were approved by The Tokyo Metropolitan Institute of Medical Science Animal Experiment Committee and were performed in accordance with the animal experimentation guidelines of The Tokyo Metropolitan Institute of Medical Science.

ELISA

Recombinant SARS-CoV N, M, E, and S proteins tagged with six histidines at the C terminus were expressed in RK13 cells by infecting with mOrVV-N-His, mOrVV-E-His, mOrVV-M-His, or mOrVV-S-His at an MOI of 5. These proteins were purified using nickel Sepharose (6 Fast Flow; GE Healthcare). His-tagged E and M proteins were further purified by SDS-PAGE. These full-length structural proteins (0.2 μg/ml, 50 μl/well) were coated onto 96-well plates at 4°C overnight. The plates were blocked with 1% BSA in PBS(−) that contained 0.5% Tween 20 and 2.5 mM EDTA, and then incubated with serial 2-fold dilutions of sera from the rabbits immunized with m8rVV-NMES or m8. After extensive washing, the plates were assayed as previously described, except that *o*-phenylenediamine was used as the substrate (17). The individual SARS-CoV structural protein-specific IgG titers are presented as the end point dilution Ab titers. The end point titer was defined as the reciprocal of the highest dilution of serum at which the absorbance at 490 nm (A_{490}) ratio (A_{490} of m8rVV-NMES-immunized serum/A_{490} of m8-immunized serum (negative control)) was greater than 2.0, as previously described (19).

In vitro neutralization assay for SARS-CoV

The neutralizing Ab titers of the sera of rabbits immunized with m8rVV-NMES or m8 were determined as previously described (17). Briefly, serial 2-fold dilutions of heat-inactivated sera were mixed with equal volumes of 200 tissue culture ID_{50} ($TCID_{50}$) of SARS-CoV and incubated at 37°C for 1 h. Vero E6 cells were then infected with 100 μl of the virus-serum mixtures in 96-well plates. After 5 days (or 6 days in the SARS-CoV challenge experiment) of infection, the neutralization titer was determined as the end point dilution of the serum at which there was 50% inhibition of the SARS-CoV-induced cytopathic effect. The method used for end point calculation was that described by Reed and Muench (20).

SARS-CoV challenge experiment

Female BALB/c mice older than the 6 mo of age (SLC) were used in this study. Four groups of eight BALB/c mice (seven mice in the vehicle-immunized group) were inoculated intradermally with either 1×10^7 PFU/body of m8, m8rVV-S, or m8rVV-NMES or 70 μl of vehicle (MEM without FCS). At 7–8 wk postimmunization, the mice were infected intranasally with 1×10^5 $TCID_{50}$/body of SARS-CoV (20 μl/mouse), as previously described (11). Four mice from each group were sacrificed 2 and 9 days later, except for the three mice of the vehicle-immunized group, which were sacrificed 2 days later. The mice were sacrificed under anesthesia and the lung, liver, small intestine, and spleen were extirpated. Aliquots of these tissues were frozen immediately at −80°C or fixed with 10% formalin. The collected blood was used for the in vitro neutralization assay. In addition, BALB/c mice were injected intradermally with 1×10^7 PFU/body of recombinant VV that expressed each structural protein of SARS-CoV (mOrVV-NHis, mOrVV-MHis, mOrVV-EHis, mOrVV-SHis) with or without LC16mOrVV-SHis (i.e., LC16mOrVV-N, -M, -E, -S alone or LC16mOrVV-N + LC16mOrVV-S, -M + LC16mOrVV-S, or -E + LC16mOrVV-S), and infected with 1×10^5 $TCID_{50}$/body of SARS-CoV more than 4 wk later. After 2 and 9 days, mice (n = 3–5 per group) were sacrificed following blood collection under anesthesia, and their lungs were extirpated. All animal experiments using mice were approved by the Animal Experiment Committee at The Institute of Medical Science, University of Tokyo, and were performed in accordance with the animal experimentation guidelines of The Institute of Medical Science, University of Tokyo.

Determination of viral titers in the organs

The SARS-CoV titers in the mouse organs were determined as previously described (11). Briefly, tissue samples (i.e., lung, liver, small intestine, and spleen) were homogenized in a 10-fold volume of Leibovitz 15 medium (Invitrogen). The homogenates were centrifuged at 2000 rpm for 10 min at 4°C. Serial 10-fold dilutions of the supernatants of these homogenates were added to Vero E6 cells seeded on 96-well plates. After 6 days of incubation, the cells were fixed with 10% formalin. Viral titer was determined as the 50% end point dilution of the homogenate that induced the cytopathic effect. The method used for end point calculation was that described by Reed and Muench (20).

Lung histopathology and inflammation scores

In accordance with a previous report (11), 10% formalin-fixed lung tissues of the SARS-CoV-infected mice were embedded in paraffin. Paraffin block sections (4-μm thickness) were stained with H&E staining. The peribronchial and perivascular scores were recorded in a blinded fashion by a pathologist. We evaluated pulmonary pathology using the histopathologic scoring systems developed by Cimolai et al. (21), in which the scoring system is weighted heavily for bronchial lesions. This scoring system allowed us to differentiate the severity of pulmonary pathology in small groups of animals. The pathology grading system consisted of a numerical score ranging from 0 to 26. In brief, each section was scored based upon a cumulative total from five categories that incorporated evaluations of the following: A) number of bronchiolar and bronchial sites affected by the periluminal infiltrate (range, 0 to 3); B) severity of the periluminal infiltrate (range, 0 to 3); C) luminal exudate severity (range, 0 to 2); D) frequency of perivascular infiltrate (range, 0 to 3); and E) severity of parenchymal pneumonia (range, 0 to 5). The accumulated numeric score was derived from the sum of the subscores: A+3(B+C)+D+E. Eosinophils were detected in tissue sections by method of Luna (22).

Extraction of total RNA and quantitative RT-PCR of cytokine or chemokine mRNA

To measure the levels of cytokine or chemokine mRNA, total RNA samples were extracted from the lungs using the RNeasy Mini kit (Qiagen). Quantitative RT-PCR was conducted with TaqMan Gene Expression assays (Applied Biosystems) using the ABI Prism 7700 and Sequence Detection System software v.1.7. The fold change in copy number of each cytokine/chemokine mRNA was revealed using the $2^{-\Delta\Delta C_T}$ method using 18 S rRNA as an endogenous calibrator.

Statistical analysis

Data are presented as mean ± SD. Statistical analysis was performed by one-way ANOVA, followed by the Dunnett or Bonferroni test. A value of $p < 0.05$ was considered to be statistically significant.

Results

Generation of recombinant VV that expresses the structural proteins of SARS-CoV

A multicistronic transgene that expresses simultaneously four structural proteins (N, M, E, and S proteins) of SARS-CoV was constructed and inserted into the HA locus of LC16m8 (m8) by homologous recombination (Fig. 1A). Expression of the transgene was placed under the control of the powerful ATI/p7.5 hybrid promoter. We screened for m8rVV-NMES using the erythrocyte agglutination assay (17), and confirmed the insertion of the transgene by PCR. Expression of the N, M, E, and S proteins in Vero E6 cells infected with m8rVV-NMES was detected by Western blot analysis. Recombinant LC16mO (mO) expressing the C-terminal histidine-tagged N, M, E or S protein (mOrVV-NHis, -MHis, -EHis, and -SHis) was generated as previously described, and used as a positive control for each protein. We also used m8rVV-S (17). As shown in Fig. 1*B*, the expression levels of the N and S proteins in the m8rVV-NMES-infected cells were high and moderate, respectively. In contrast, the expression levels of the M and E proteins in m8rVV-NMES-infected cells were weaker than those in mOrVV-MHis- and mOrVV-EHis-infected cells. The M protein in the m8rVV-NMES-infected cells was 20 kDa, whereas that in the mOrVV-MHis-infected cells was observed as forms of ~20 kDa (nonglycosylated form) and 25 kDa (glycosylated form) (23). Furthermore, we investigated the cellular localizations of these structural proteins by indirect immunofluorescence (Fig. 1*C*). In m8rVV-NMES-infected cells, all of the SARS-CoV proteins were localized in the perinuclear regions. In particular, the localization of the N protein in m8rVV-NMES-infected cells was different from that in mOrVV-NHis-infected cells, in which the N-His protein was found diffusely in the cytoplasm. VLPs are formed by the assembly of structural proteins in the cytoplasm, followed by release into the culture medium. By infecting m8rVV-NMES into RK13 cells, we confirmed

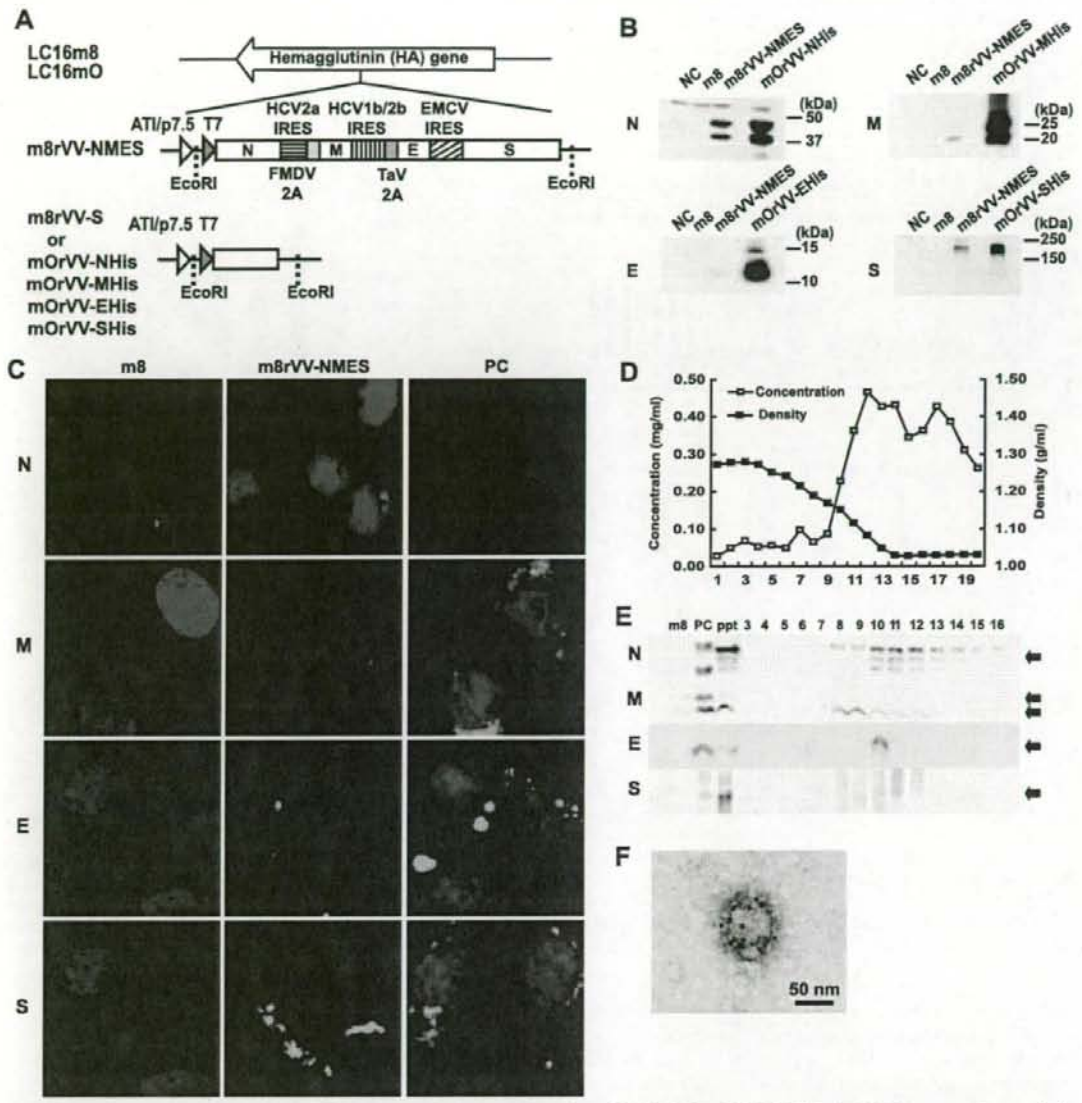

FIGURE 1. Construction of recombinant VV that express four structural proteins of SARS-CoV (m8rVV-NMES). *A*, DNA fragments that encode the SARS-CoV N, M, E, and S proteins were ligated with the internal ribosomal entry site sequence of hepatitis C virus (2a and 1b/2b) and fused with the 2A sequences of foot and mouth disease virus (FMDV) and *Thosea asigna* virus (TaV) or encephalomyocarditis (EMCV). After digestion with *Eco*RI, the DNA fragment was inserted into the pBMSF vector, and the resultant plasmid was designated as pBMSF-NMES. *Pvu*I-linearized pBMSF-NMES was used for homologous recombination into the HA locus of the LC16m8 genome. Recombinant mO that expressed the SARS-CoV N, M, E, or S protein was generated (mOrVV-NHis, -MHis, -EHis, and -SHis) as described in *Materials and Methods*. *B*, Vero E6 cells were infected with m8rVV-NMES or m8. Uninfected Vero E6 cells were used as a negative control (NC). Structural proteins mOrVV-NHis, mOrVV-MHis, mOrVV-EHis, and mOrVV-SHis were used as positive controls. SARS-CoV structural proteins were detected using rabbit polyclonal Abs and donkey anti-rabbit IgG polyclonal Abs, which were conjugated with HRP. The lane between m8rVV-NMES and the mOrVV-N, mOrVV-M, mOrVV-E, and mOrVV-S samples was left empty, to exclude the possibility of leakage of sample solution between lanes. *C*, Vero E6 cells were infected with m8rVV-NMES at an MOI of 5 at 30°C for 4 h. The SARS-CoV proteins in the fixed cells were visualized with the polyclonal Abs against the N, M, or E protein or mAb against the S protein (designated as 13B8). Nuclei were stained with DAPI). Structural proteins mOrVV-NHis, mOrVV-MHis, mOrVV-EHis, and mOrVV-SHis were used as positive controls (PC). *D*, The VLPs were isolated from the culture supernatants of RK13 cells infected with m8rVV-NMES at an MOI of 5 for 48 h at 30°C. After sucrose gradient centrifugation, 20 fractions were collected. *E*, Equal amounts of the gradient fractions (nos. 3–16) were examined by Western blot analyses. m8, m8-infected RK13 cell lysate; ppt, m8rVV-NMES-infected RK13cell lysate; PC, RK13 cell lysates infected with mOrVV-NHis, mOrVV-MHis, mOrVV-EHis, or mOrVV-SHis. *F*, A concentrated culture supernatant was subjected to transmission electron microscopy. VLPs were probed with polyclonal Ab against the S protein and incubated with 5-nm gold-conjugated anti-rabbit IgG.

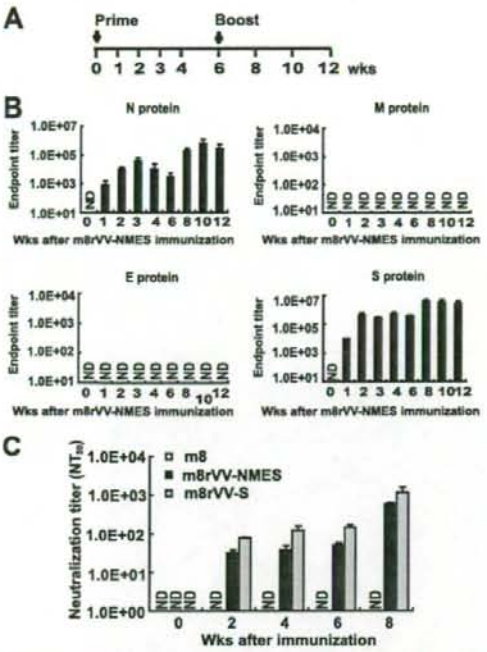

FIGURE 2. Immunogenicity of m8rVV-NMES in rabbits. *A*, New Zealand White rabbits ($n = 3$) were inoculated intradermally with 10^8 PFU/body of m8rVV-NMES or m8 at 0 and 6 wk. Blood samples were collected at the indicated time points. *B*, Induction of serum IgG specific for the four structural proteins of SARS-CoV. The individual SARS-CoV structural protein-specific IgG titers are presented as the end point dilution Ab titers. The end point titer was defined as the reciprocal of the highest dilution of serum at which the absorbance at 490 nm (A_{490}) ratio (A_{490} of m8rVV-NMES-immunized serum/A_{490} of m8-immunized serum (negative control)) was greater than 2.0. *C*, Induction of neutralizing Abs against SARS-CoV. The neutralization titer of m8rVV-NMES-immunized rabbit sera was defined as the end point dilution of the serum at which there was 50% inhibition (NT_{50}) of the SARS-CoV-induced cytopathic effect. Immunization with m8rVVs or m8 was conducted using the schedule described in Fig. 3*A*. ND, Not detectable.

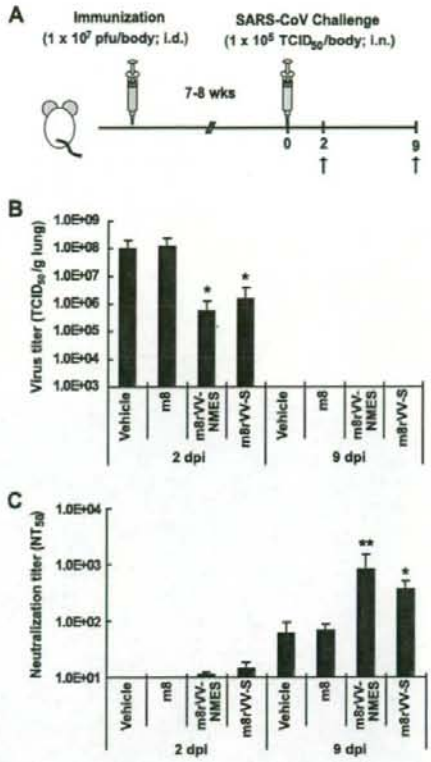

FIGURE 3. SARS-CoV challenge to BALB/c mice immunized with m8rVV-NMES or m8rVV-S. *A*, Four groups of eight BALB/c mice (seven mice in the vehicle-immunized group) were inoculated intradermally with m8rVV-NMES, m8rVV-S, m8, or vehicle and challenged 7–8 wk later with 1×10^5 $TCID_{50}$/body of SARS-CoV delivered via the intranasal route. Blood and lung tissues samples were collected at the indicated time points. *B*, After 2 and 9 days, the titers of SARS-CoV in the lungs of four mice in each group (except for three mice of the vehicle-immunized group, which were examined 2 days later) were determined. Virus titers are expressed as $\log_{10}$ $TCID_{50}$/g of tissue. *C*, At 2 and 9 days after SARS-CoV infection, the serum neutralization titers of all groups were measured as described in *Materials and Methods*. *, $p < 0.05$; **, $p < 0.01$, as compared with both the vehicle- and m8-immunized groups.

the formation of VLPs in the culture medium. After sucrose gradient centrifugation, 20 fractions (500 μl each) were collected (Fig. 1*D*). The four SARS-CoV structural proteins were monitored by Western blot analysis. As shown in Fig. 1*E*, fraction number 10 contained all the SARS-CoV proteins, and the buoyant density of this fraction was ~1.15 g/ml, a value that is consistent with previous reports (18, 24, 25). Moreover, we confirmed the formation of VLPs in the concentrated culture supernatant using scanning electron microscopy and immunogold-labeling with the anti-S protein polyclonal Ab. The particles were 70–100 nm in diameter, which is consistent with the sizes as reported previously (18, 24, 25). The particles were positively stained with immunogold (Fig. 1*F*).

Induction of Abs specific for SARS-CoV structural proteins in rabbits immunized with m8rVV-NMES

To investigate the immunogenicity of m8rVV-NMES, 1×10^8 PFU/body of either m8rVV-NMES or m8, its parental strain, was inoculated intradermally on the backs of New Zealand White rabbits at 0 and 6 wk (Fig. 2*A*). Rabbit antisera specific for the full-length structural proteins of SARS-CoV were detected by ELISA (Fig. 2*B*). In agreement with previous reports (26–28), the N and S proteins both exhibited strong immunogenicity in rabbits. IgG-specific for the N or S protein was induced as early as 1 wk after m8rVV-NMES immunization, and the titer exceeded 1:10000 2 wk later. The titers of Abs against the N and S proteins were dramatically increased by booster immunization with m8rVV-NMES. It was also observed that the Ab titer of the N protein, but not that of the S protein, decreased after reaching the peak titer. Immunization with m8rVV-NMES did not induce Abs specific for the E and M proteins, even after booster immunization (Fig. 2*B*). The antigenicity of the purified E and M proteins coated onto the ELISA plates was confirmed using each rabbit anti-E or anti-M peptide Ab (data not shown). Therefore, we believe that the lack of induction of Abs specific for the E and M proteins in the rabbit sera results from the poor immunogenicity and lower expression levels of these proteins.

Induction of SARS-CoV-neutralizing serum Abs in rabbits by immunizing with m8rVV-NMES

We determined the neutralization titers against SARS-CoV using the same rabbit antisera. The neutralization titer was ~1:30

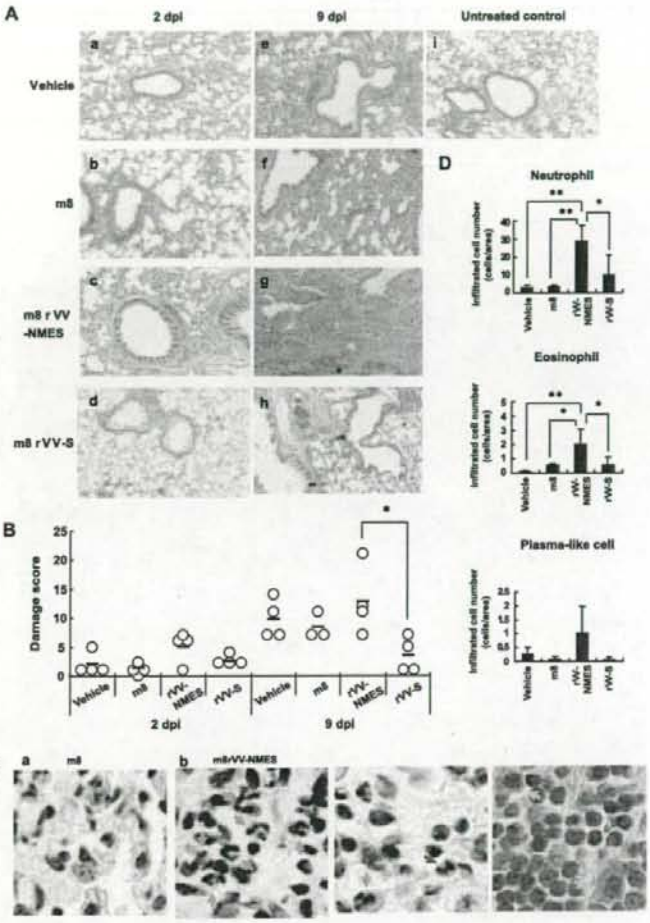

FIGURE 4. Pulmonary histopathology of m8rVV-S-preimmunized BALB/c mice after SARS-CoV challenge. At 7–8 wk after immunization with m8rVV-NMES, m8rVV-S, m8, or vehicle, the mice were infected intranasally with 1×10^5 $TCID_{50}$/body of SARS-CoV. *A*, Four mice from each group (three mice from the vehicle-immunized group were killed 2 days later) were sacrificed 2 and 9 days later. Extirpated lung tissues were fixed with 10% formalin and embedded in paraffin. Paraffin block sections (4-μm thickness) were stained with H&E staining. Histopathologic sections were prepared for vehicle-immunized mice at 2 days postinfection (dpi) (a) and 9 dpi (e), m8-immunized mice at 2 dpi (b) and 9 dpi (f), m8rVV-NMES-immunized mice at 2 dpi (c) and 9 dpi (g), m8rVV-S-immunized mice at 2 dpi (d) and 9 dpi (h), and uninfected mice (i). *B*, The degree of pulmonary inflammation was determined in a blinded fashion on a subjective 27-point scale (0, minimal inflammation; 26, massive inflammation) as described in *Materials and Methods*. Each symbol represents an individual mouse. *, $p < 0.05$. *C*, Representative lung sections from m8-immunized mice (a) and m8rVV-NMES-immunized mice (b) after staining with Luna method (for eosinophils and neutrophils) and H&E (for plasma cells). Arrows indicate neutrophils (yellow), eosinophils (red), and plasma-like cells (green). *D*, The numbers of neutrophils, eosinophils, and plasma-like cells that infiltrated the lung were counted using Luna method and H&E staining. Data are mean ± SD for $n = 5$ mice. Fields viewed at a magnification of ×400. *, $p < 0.05$; **, $p < 0.01$, for significant differences evaluated using the Bonferroni test.

(range, 1:25 to 1:36) after 2 wk, and was sustained for 6 wk (Fig. 2*C*). Booster immunization with m8rVV-NMES further increased the neutralization titer more than 10-fold 2 wk later. These values are somewhat lower than those induced by m8rVV-S in our previous report (17). In contrast, the antisera from rabbits immunized with m8 did not exhibit any neutralizing activity against SARS-CoV (Fig. 2*C*).

SARS-CoV challenge of BALB/c mice having prior immunization with m8rVV-NMES or m8rVV-S

As m8rVV-NMES and m8rVV-S could induce high levels of neutralizing Abs against SARS-CoV (Fig. 2*C*), we investigated the influences of m8rVV-NMES and m8rVV-S on SARS-CoV challenge of BALB/c mice (Fig. 3*A*). The m8rVV-NMES and m8rVV-S constructs were inoculated intradermally on the backs of BALB/c mice at 1×10^7 PFU/body. At 7–8 wk after this single immunization, the mice were infected intranasally with SARS-CoV at 1×10^5 $TCID_{50}$/body. After 2 and 9 days, the lung, liver, small intestine, and spleen were extirpated from the mice under anesthesia, and the SARS-CoV titers were measured. As shown in Fig. 3*B*, 200- and 100-fold reductions in pulmonary virus titers were observed in the m8rVV-NMES-immunized and m8rVV-S-immunized groups 2 days after infection. The virus titers in the lungs of the m8rVV-NMES-immunized and m8rVV-S-immunized groups were 5.40×10^5 and 1.52×10^6 $TCID_{50}$/g of lung, respectively. In contrast, the vehicle-immunized and LC16m8-immunized groups exhibited virus titers of 1.07×10^8 and 1.18×10^8 $TCID_{50}$/g of lung, respectively. The virus was not detected in the lungs of any group 9 days later, as reported previously (11, 15). In contrast, virus titers in other organs, including liver, small intestine, and spleen, were lower than that of the detection limit 2 and 9 days after infection (data not shown).

We also measured the neutralization titers in these mice sera 2 and 9 days after SARS-CoV infection (Fig. 3*C*). Two days postinfection, the neutralization titers of the m8rVV-NMES-immunized and m8rVV-S-immunized groups were 1:11.1 ± 1.01 and 1:14 ± 3.94, respectively, whereas those of the negative control groups were below the limit of detection. At 9 days postinfection, the serum neutralization titers of m8rVV-NMES-immunized and m8rVV-S-immunized groups had increased to 1:838.0 ± 681.0 and 1:367.9 ± 132.1, respectively. In contrast, the serum neutralizing titers of the vehicle-immunized and m8-immunized groups were 1:59.7 ± 35.4 and 1:67.8 ± 18.6, respectively. These results suggest that both the m8rVV-NMES- and m8rVV-S-immunized groups could elicit neutralizing Abs against SARS-CoV and alleviate SARS-CoV infection.

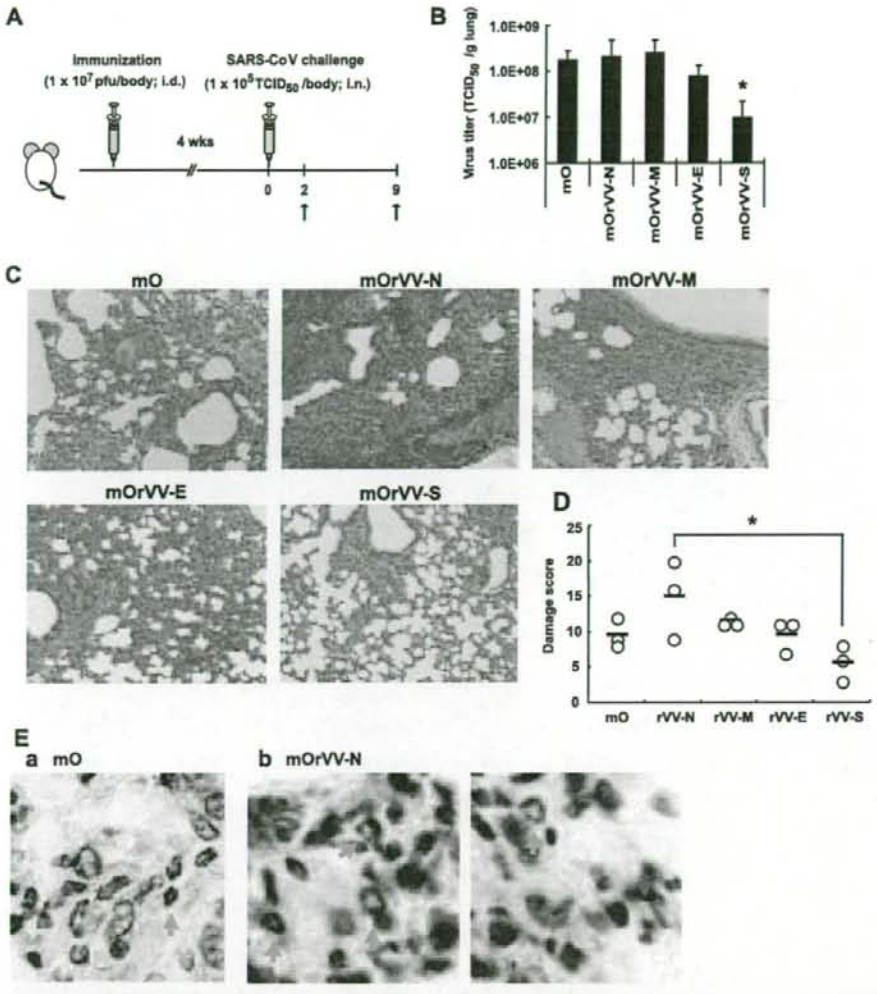

FIGURE 5. Identification of SARS-CoV structural protein implicated in severe pulmonary inflammation. *A*, Five groups of six BALB/c mice were inoculated intradermally with mOrVV-NHis, mOrVV-MHis, mOrVV-EHis, mOrVV-SHis, or mO and challenged 4 wk later with 1×10^5 $TCID_{50}$/body of SARS-CoV via the intranasal route. *B*, After 2 days, the titers of SARS-CoV in the lungs of three mice in each group were determined. Virus titers are expressed as $\log_{10}$ $TCID_{50}$/g of tissue. *, $p < 0.05$, as compared with the mO-immunized group using the Dunnett test. *C*, Histopathologic findings for all the groups 9 days after SARS-CoV infection. Extirpated lung tissues were fixed with 10% formalin and embedded in paraffin. Paraffin block sections (4-μm thickness) were subjected to H&E staining. *D*, The degree of pulmonary inflammation was determined in a blinded fashion on a subjective 27-point scale (0, minimal inflammation; 26, massive inflammation). Each symbol represents an individual mouse. *, $p < 0.05$. *E*, Representative lung sections from mO-immunized mice (a) and mOrVV-N-immunized mice (b) after staining with Luna method (for eosinophils and neutrophils). Arrows indicate neutrophils (yellow) and eosinophils (red).

Histopathologic findings in the lungs of m8rVVs-immunized BALB/c mice after SARS-CoV infection

We performed histopathologic analyses of lung tissues. Two days after SARS-CoV infection, the vehicle-, m8-, and m8rVV-S-immunized groups showed only slight pulmonary inflammation (Fig. 4*A*, a, b, and d), whereas the m8rVV-NMES-immunized group showed infiltration of lymphocytes into the areas surrounding the bronchi and slight thickening of the alveolar epithelium (Fig. 4*A*, c). We scored pulmonary inflammation in all the groups 2 days after SARS-CoV infection as follows (Fig. 4*B*): in the m8rVV-NMES-immunized group, 5.00 ± 2.71; in the vehicle-immunized group, 2.00 ± 2.00; in the m8-immunized group, 1.33 ± 0.82; and in the m8rVV-S-immunized group, 2.50 ± 1.00. At 9 days postinfection, the vehicle-, m8-, and m8rVV-NMES-immunized groups exhibited severe pulmonary inflammation, i.e., infiltration of inflammatory cells and thickening of alveolar epithelia (Fig. 4*A*, e, f, and g). In contrast, the m8rVV-S-immunized group showed only slight pulmonary inflammation (Fig. 4*A*, h). As shown in Fig. 4*B*, the pulmonary inflammation score for the m8rVV-NMES-immunized group (12.75 ± 2.87) 9 days after SARS-CoV infection was significantly higher than that for the m8rVV-S-immunized group (3.50 ± 3.00). In contrast, this score was comparable to those obtained for the vehicle-immunized and m8-immunized groups (9.75 ± 2.87 and

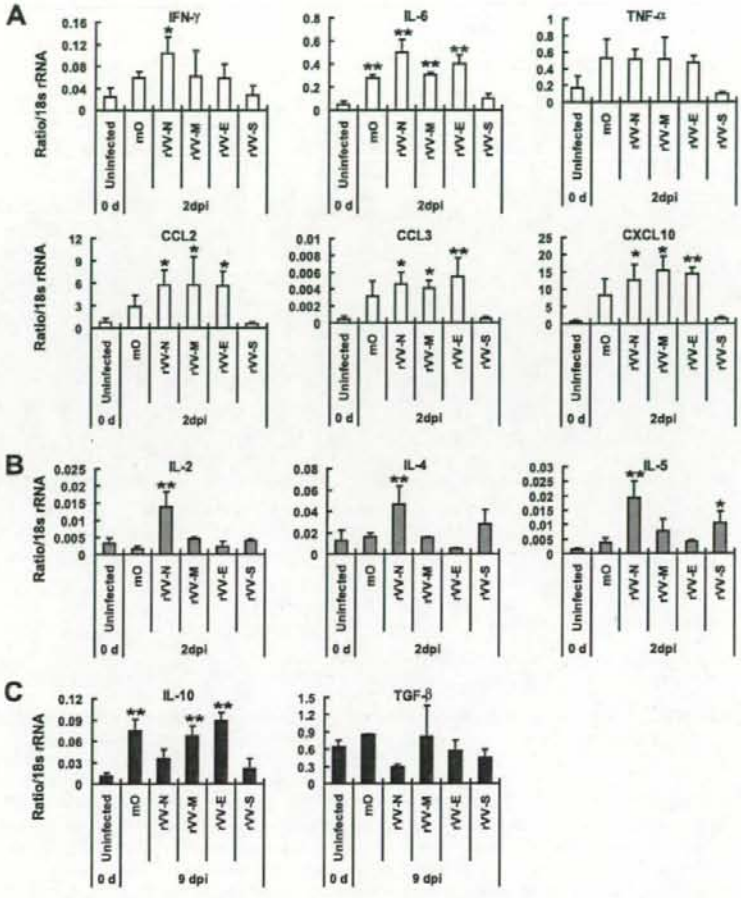

FIGURE 6. Cytokine profiles of the lungs of BALB/c mice preimmunized with each SARS-CoV structural protein and challenged with SARS-CoV. Three mice from each group were sacrificed 2 and 9 days postinfection. The total RNA of the lung was extracted. Quantitative RT-PCR was conducted as described in *Materials and Methods*. The fold change in copy number of each cytokine or chemokine mRNA was calculated by the $2^{-\Delta\Delta Ct}$ method using 18 S rRNA as an endogenous calibrator. *, $p < 0.05$; **, $p < 0.01$, as compared with the uninfected control group using the Bonferroni test. *A*, The levels of mRNA for proinflammatory cytokines and chemokines 2 days after SARS-CoV infection. *B*, The mRNA expression levels of cytokines related to T cell activation 2 days after SARS-CoV infection. *C*, The mRNA expression levels of anti-inflammatory cytokines 9 days after SARS-CoV infection.

8.33 ± 2.31, respectively). The m8rVV-NMES-immunized group exhibited as severe inflammation as the control groups, although m8rVV-NMES contains the S protein and protects as well as m8rVV-S against SARS-CoV infection. In addition, marked infiltration of neutrophils, eosinophils, plasma-like cells, and lymphocytes was observed in the m8rVV-NMES-immunized group, as compared with the control groups, after SARS-CoV infection (Fig. 4*C*, b and *D*).

These results suggest that the severe pulmonary inflammation seen in m8rVV-NMES-immunized mice after SARS-CoV infection results from host immune responses rather than a direct cytopathic effect of SARS-CoV, because the virus titers for all the group were negligible 9 days after SARS-CoV infection and the virus titer of the m8rVV-NMES-immunized group was significantly decreased 2 days postinfection.

Identification of the factor that results in the exacerbation of pulmonary inflammation in m8rVV-NMES-immunized BALB/c mice after SARS-CoV infection

We hypothesized that the severe pulmonary inflammation seen in the m8rVV-NMES-immunized mice resulted from the host immune responses to SARS-CoV components expressed by m8rVV-NMES. This notion was supported by the observation of negligible virus titers 9 days after SARS-CoV infection. Therefore, we investigated the influence of recombinant VV expressing each structural protein of SARS-CoV (mOrVV-NHis, mOrVV-MHis, mOrVV-EHis, and mOrVV-SHis) on subsequent intranasal infection with SARS-CoV. BALB/c mice were immunized with mOrVV-NHis, -MHis, -EHis, and -SHis at 1×10^7 PFU/body, and 4 wk later infected intradermally with 1×10^5 $TCID_{50}$ of SARS-CoV (Fig. 5*A*). After 2 and 9 days, three mice from each group were sacrificed following blood collection under anesthesia, and their lungs were extirpated. Consistent with earlier results, a significant reduction of pulmonary virus titer was observed after 2 days in only the mOrVV-SHis-immunized group (Fig. 5*B*). In contrast, immunization with the other SARS-CoV structural proteins, including the N, M, and E proteins, did not confer protection against the subsequent SARS-CoV infection. As shown in Fig. 5*C*, the alleviation of pulmonary inflammation was also observed in the mOrVV-SHis-immunized group. Severe infiltration of lymphocytes and thickening of the alveolar epithelia were observed in the lung tissues of the mOrVV-NHis-immunized mice 9 days after SARS-CoV infection (Fig. 5*C*). The pulmonary damage in the mOrVV-NHis-immunized mice (15.00 ± 5.56) was significantly more severe than that in the mOrVV-SHis-immunized mice (5.67 ± 2.52) (Fig. 5*D*). However, there were no significant differences among the other groups. Furthermore, infiltration of neutrophils, eosinophils, and lymphocytes was observed in the

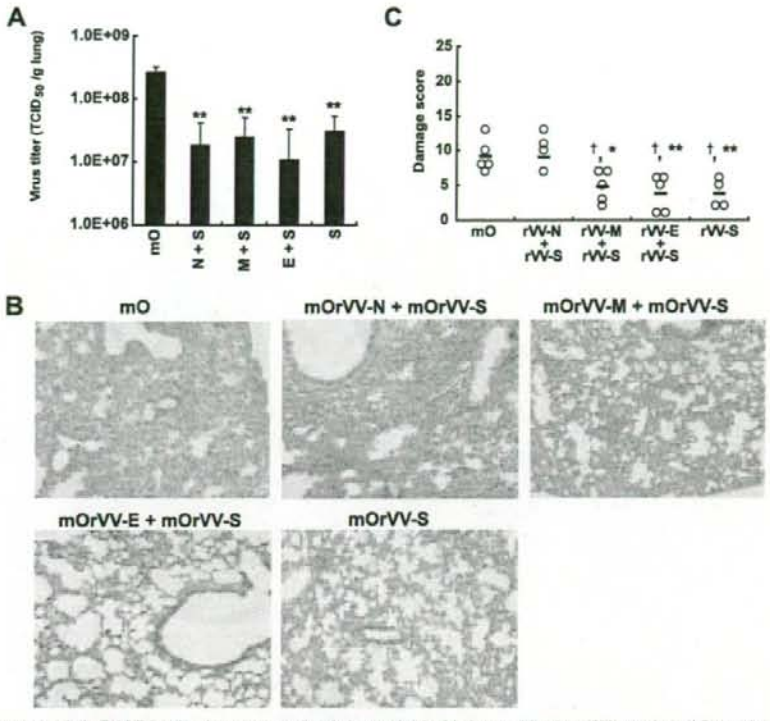

FIGURE 7. Severe pneumonia in BALB/c mice that were previously immunized with the combination of N protein and S protein of SARS-CoV. *A*, Five groups of BALB/c mice ($n = 8$–10 per group) were inoculated intradermally with the combinations of mOrVV-NHis and mOrVV-SHis (mOrVV-N+S), mOrVV-MHis and mOrVV-SHis (mOrVV-M+S), mOrVV-EHis and mOrVV-SHis (mOrVV-E+S), mOrVV-SHis, and mO, and challenged 7 wk later with 1×10^5 $TCID_{50}$/body of SARS-CoV via the intranasal route. After 2 days, the titers of SARS-CoV in the lungs of $n = 3$–5 mice from each group were determined. Virus titers are expressed as $\log_{10}$ $TCID_{50}$/g of tissue. *, $p < 0.05$, **, $p < 0.01$, as compared with the mO-immunized group using the Bonferroni test. *B*, Histopathologic findings for all the groups 9 days after SARS-CoV infection. Extirpated lung tissues were fixed with 10% formalin and embedded in paraffin. Paraffin block sections (4-μm thickness) were subjected to H&E staining. *C*, The degree of pulmonary inflammation was determined in a blinded fashion on a subjective 27-point scale (0, minimal inflammation; 26, massive inflammation). Each symbol represents an individual mouse. †, $p < 0.05$; ‡, $p < 0.01$, as compared with the mO-immunized group using the Bonferroni test. *, $p < 0.05$; **, $p < 0.01$, as compared with the mOrVV-N + S-immunized group using the Bonferroni test.

mOrVV-NHis-immunized mice after SARS-CoV infection (Fig. 5*E*, b), although the extent of infiltration of these cells into the lungs of these mice was somewhat lower than that observed in the m8rVV-NMES-immunized mice after SARS-CoV infection (Fig. 4*D*). This may explain the observed differences in the histopathologic findings for the mOrVV-NHis-immunized mice and m8rVV-NMES-immunized mice.

Pulmonary cytokine responses of SARS-CoV-infected BALB/c mice previously immunized with recombinant VV expressing each structural protein of SARS-CoV

To elucidate the reason for the severe pulmonary inflammation observed in the mOrVV-NHis-immunized mice after SARS-CoV infection, we measured by quantitative RT-PCR the mRNA levels for various cytokines and chemokines in the lungs of BALB/c mice preimmunized with mOrVV-NHis, -MHis, -EHis, -SHis, or mO. Several proinflammatory cytokine and chemokine mRNAs, including those for IL-6, CXCL10, CCL2, and CCL3, were increased in all the groups, with the exception of the mOrVV-SHis group, 2 days after SARS-CoV infection (Fig. 6*A*). In contrast, the mOrVV-SHis-immunized group showed low levels of mRNA expression for these proinflammatory cytokines or chemokines, especially IL-6, resulting in reduced lung pathology after immunization. The mRNA levels for IFN-γ, IL-2, IL-4, and IL-5 were highest in the mOrVV-NHis-immunized group (Fig. 6, *A* and *B*). None of the other groups showed up-regulation of these cytokines, with the exception of the IL-5 mRNA level in the mOrVV-SHis-immunized group. Furthermore, the mRNA expression levels of anti-inflammatory cytokines (IL-10 and TGF-β) in the mOrVV-NHis-immunized group were markedly lower than expression levels in any of the other groups, which exhibited high virus titers, and were comparable to those of the mOrVV-SHis group, in which pulmonary inflammation was alleviated (Fig. 6*C*).

Verification of exacerbating effect of prior immunization with N protein in SARS-CoV-infected Balb/c mice

To verify the exacerbating effect of N protein immunization, we investigated the pulmonary virus titers and histopathology in BALB/c mice that were previously immunized with the combination of mOrVV-N and mOrVV-S (mOrVV-N+S-immunized group) 2 and 9 days after SARS-CoV infection, and compared them to those of all other groups, including the mO-, mOrVV-M+S-, mOrVV-E+S-, and mOrVV-S-immunized groups. The mOrVV-N+S-immunized group showed significantly decreased pulmonary virus titers compared with the mO-immunized group (Fig. 7*A*). However, the mOrVV-N+S-immunized group exhibited as

severe pneumonia as the mO-immunized group (Fig. 7, *B* and *C*). In contrast, both the mOrVV-M+S-immunized group and the mOrVV-E+S-immunized group were protected against SARS-CoV infection to the same extent as the mOrVV-S-immunized group (Fig. 7, *A–C*).

Discussion

SARS-CoV is newly identified as an agent of SARS. However, the detailed mechanism by which SARS-CoV causes severe pneumonia remains unclear. The uncontrolled release of immune mediators has been implicated in the pathogenesis of SARS, whereas the cytokine profiles of SARS patients have not elucidated the cause the pneumonia owing to their diversity. It seems likely that the diverse cytokine profiles noted among adult SARS patients are related to patient anamnesis.

In the present study, we observed severe pulmonary inflammation in m8rVV-NMES-immunized BALB/c mice 9 days after SARS-CoV infection (Fig. 4*A*, g), even though the initial virus titer was significantly lower than those of the control groups, which included vehicle- and m8-immunized mice (Fig. 3*B*). The severity of pulmonary inflammation did not correlate with the virus titer in the m8rVV-NMES-immunized mice, in contrast to the correlations observed for the vehicle-, m8-, and m8rVV-S-immunized groups. We identified the N protein of SARS-CoV as the cause of the severe pneumonia observed during SARS-CoV infection (Fig. 5, *C* and *D*, and 7, *B* and *C*). To date, no studies have been reported to our knowledge regarding SARS patients with severe pneumonia who were previously immunized with either SARS-CoV or a highly related species. In contrast, there are several reports of antisera against human CoV (229E and OC43) and host factor IL-11 cross-reacting with the SARS-CoV Ag (29, 30). Furthermore, the N protein of SARS-CoV has been shown to induce both cellular and humoral immune responses (31–33). Taken together, these results raise the possibility that a percentage of SARS patients already possess the adaptive immune response elements that can interact with SARS-CoV components, including the N protein, and that their adaptive immune response may be involved in the exacerbation of pneumonia. The temporal changes in immune response and the pathogenesis after SARS-CoV infection of an animal model that had previously been immunized with SARS-CoV components are not well understood, as almost all the previous studies reported only protection within a few days of SARS-CoV infection (34–39). In the present study, we demonstrate that mOrVV-NHis-immunized mice after SARS-CoV infection exhibit an imbalance between T cell activation (high expression levels of IFN-γ, IL-2, IL-4, and IL-5) and subsequent suppression (low expression levels of IL-10 and TGF-β), as well as high-level production of proinflammatory cytokines (IL-6 and TNF-α) and chemokines (CCL2, CCL3, and CXCL10). Jiang et al. (40) reported elevation of CXCL10 or IP-10 production in the pneumocytes, $CD3^+$ T cells, and monocytes and macrophages of the lungs of patients with SARS. CXCL10 may be responsible for the infiltration of activated T cells and monocytes or macrophages, which is a pathologic finding in SARS patients (41–43). It has been reported that elevated expression of monocyte or macrophage activation factors (CCL2 and CCL3) was observed in SARS patients (8, 44). Furthermore, the highest expression of IL-6 in mOrVV-NHis-immunized mice is reasonable (Fig. 6*A*), as the elevation of IL-6 levels is considered one of the causes in the severe pneumonia of SARS patients. Zhang et al. (45) reported recently the molecular mechanism of IL-6 expression induction by the N protein of SARS-CoV. In contrast, both IL-10 and TGF-β play important roles in suppressing inflammatory responses (46). Thus, the reduced production of both anti-inflammatory cytokines in the mOrVV-NHis-immunized mice after SARS-CoV infection may be related to the severity of the pulmonary inflammation in these mice. Weingartl et al. (47) and Czub et al. (48) reported that immunization with S protein expressing-recombinant modified VV Ankara (rMVA-S) induced stronger inflammatory responses and focal necrosis in liver tissues after SARS-CoV challenge than in control animals. However, the precise mechanism underlying this liver inflammation has not been clarified. Feline infectious peritonitis virus, which is another member of the coronavirus family, exhibits enhanced infection into monocytes or macrophages through virus-specific Ab binding to the Fc receptors of these cells and causes enhanced inflammation (49). It has also been reported for dengue virus that secondary infection with a different genotype results in more severe symptoms, including dengue hemorrhagic fever and dengue shock syndrome. The exacerbation of this symptom is also positively associated with pre-existing Abs with specificity for dengue virus (50). In the case of SARS-CoV, Ab-dependent enhancement of infection has not been reported previously. We hypothesized that the severe pneumonia observed in mOrVV-NHis-immunized mice after SARS-CoV infection does not result from Ab-dependent enhancement because the virus titers in the mouse lungs 9 days later were below the detection limit. Deming et al. (51) reported recently the intensive infiltration of eosinophils as well as lymphocytes after SARS-CoV infection of aged BALB/c mice previously immunized with the N protein of SARS-CoV. It has also been reported that immunization with formalin-inactivated respiratory syncytial virus vaccine and VV that expresses the G glycoprotein of respiratory syncytial virus correlates with the augmentation of Th2-type immune responses and enhanced pulmonary disease (52, 53). Therefore, the authors speculated that the Th2-biased responses of vaccinated hosts after SARS-CoV infection might aggravate pulmonary inflammation, although the main host response remains unknown. In contrast, our current data suggest that N protein-immunized mice exhibit activation of both Th1 and Th2 responses after SARS-CoV infection. In agreement with our data, Jin et al. (54) have demonstrated that prior immunization with N protein generates stronger Ag-specific Th1 and Th2 responses than immunization with M or E protein. In addition, we demonstrate the suppression of anti-inflammatory cytokine responses in N protein-immunized mice. Interestingly, Shi et al. (55) demonstrated that coinjection of M protein with N protein not only enhanced the production of Th1 cytokines (IFN-γ and IL-2), but also reduced the rates of mortality and pathologic change in SARS-CoV-infected voles. These results suggest that further studies, including epitope analysis, are required to reveal the precise mechanism underlying the severe pulmonary inflammation that results from SARS-CoV infection of BALB/c mice immunized with the N protein of SARS-CoV.

In contrast, intradermal immunization of aged BALB/c mice with m8rVV-S at 1×10^7 PFU/body significantly reduced the pulmonary virus titer 2 days after SARS-CoV infection (Fig. 3*B*). Furthermore, the m8rVV-S-immunized group exhibited alleviation of the pulmonary histopathology, as compared with both control groups after 9 days. To date, various types of SARS vaccine, including recombinant vaccines, inactivated vaccines, and DNA vaccine, have been reported (34–39). There are only a few reports on the effect of a single immunization with recombinant SARS vaccines, namely SARS-CoV S protein-expressing vaccines based on rabies virus (56), vesicular stomatitis virus (39), and adeno-associated virus (57). It is noteworthy that a single i.m. immunization with recombinant adeno-associated virus that expresses the receptor-binding domain of S protein conferred long-term protection against SARS-CoV infection (57). In the present study, we also show that a single immunization with m8rVV-S reduces viral load and improves the histopathologic findings in the lungs of BALB/c

mice infected with high-titer (1×10^5 $TCID_{50}$/body) SARS-CoV, although a relatively low titer of SARS-CoV was used in the previous study conducted by Du et al. (57). These results suggest that the systemic immune responses induced by a single immunization with SARS vaccine successfully protect the animal model against intranasal SARS-CoV infection.

In summary, we demonstrate that the immunization of BALB/c mice with the N protein of SARS-CoV causes severe pulmonary inflammation upon subsequent SARS-CoV infection, probably via the imbalance created between T cell activation and suppression, as well as by massive proinflammatory cytokine production. These results provide new insights into the mechanisms involved in the pathogenesis of SARS and help in the development of safe vaccines.

Acknowledgments

We are grateful to Dr. Ryuichi Miura (University of Tokyo) for arranging the SARS-CoV challenge experiment. We are also grateful to Iyo Kataoka (Institute of Medical Science, University of Tokyo). We thank Dr. Masahiro Shuda of the University of Pittsburgh for helpful discussions. We also thank Dr. Tetsuya Mizutani and Dr. Shigeru Morikawa (Department of Virology I, National Institute of Infectious Diseases) for providing antisera from rabbits immunized with the M protein peptide and inactivated SARS-CoV particles.

Disclosures

The authors have no financial conflict of interest.

References

1. Drosten, C., S. Gunther, W. Preiser, S. van der Werf, H. R. Brodt, S. Becker, H. Rabenau, M. Panning, L. Kolesnikova, R. A. Fouchier, et al. 2003. Identification of a novel coronavirus in patients with severe acute respiratory syndrome. *N. Engl. J. Med.* 348: 1967–1976.
2. Ksiazek, T. G., D. Erdman, C. S. Goldsmith, S. R. Zaki, T. Peret, S. Emery, S. Tong, C. Urbani, J. A. Comer, W. Lim, et al. 2003. A novel coronavirus associated with severe acute respiratory syndrome. *N. Engl. J. Med.* 1953–1966.
3. Peiris, J. S., S. T. Lai, L. L. Poon, Y. Guan, L. Y. Yam, W. Lim, J. Nicholls, W. K. Yee, W. W. Yan, M. T. Cheung, et al. 2003. Coronavirus as a possible cause of severe acute respiratory syndrome. *Lancet* 361: 1319–1325.
4. Rota, P. A., M. S. Oberste, S. S. Monroe, W. A. Nix, R. Campagnoli, J. P. Icenogle, S. Penaranda, B. Bankamp, K. Maher, M. H. Chen, et al. 2003. Characterization of a novel coronavirus associated with severe acute respiratory syndrome. *Science* 300: 1394–1399.
5. Li, W., M. J. Moore, N. Vasilieva, J. Sui, S. K. Wong, M. A. Berne, M. Somasundaran, J. L. Sullivan, K. Luzuriaga, T. C. Greenough, et al. 2003. Angiotensin-converting enzyme 2 is a functional receptor for the SARS coronavirus. *Nature* 426: 450–454.
6. Hamming, I., W. Timens, M. L. Bulthuis, A. T. Lely, G. J. Navis, and H. van Goor. 2004. Tissue distribution of ACE2 protein, the functional receptor for SARS coronavirus. A first step in understanding SARS pathogenesis. *J. Pathol.* 203: 631–637.
7. Jones, B. M., E. S. Ma, J. S. Peiris, P. C. Wong, J. C. Ho, B. Lam, K. N. Lai, and K. W. Tsang. 2004. Prolonged disturbances of in vitro cytokine production in patients with severe acute respiratory syndrome (SARS) treated with ribavirin and steroids. *Clin. Exp. Immunol.* 135: 467–473.
8. Wong, C. K., C. W. Lam, A. K. Wu, W. K. Ip, N. L. Lee, I. H. Chan, L. C. Lit, D. S. Hui, M. H. Chan, S. S. Chung, and J. J. Sung. 2004. Plasma inflammatory cytokines and chemokines in severe acute respiratory syndrome. *Clin. Exp. Immunol.* 136: 95–103.
9. Rowe, T., G. Gao, R. J. Hogan, R. G. Crystal, T. G. Voss, R. L. Grant, P. Bell, G. P. Kobinger, N. A. Wivel, and J. M. Wilson. 2004. Macaque model for severe acute respiratory syndrome. *J. Virol.* 78: 11401–11404.
10. Osterhaus, A. D., R. A. Fouchier, and T. Kuiken. 2004. The aetiology of SARS: Koch's postulates fulfilled. *Philos. Trans. R. Soc. Lond B Biol. Sci.* 359: 1081–1082.
11. Subbarao, K., J. McAuliffe, L. Vogel, G. Fahle, S. Fischer, K. Tatti, M. Packard, W. J. Shieh, S. Zaki, and B. Murphy. 2004. Prior infection and passive transfer of neutralizing antibody prevent replication of severe acute respiratory syndrome coronavirus in the respiratory tract of mice. *J. Virol.* 78: 3572–3577.
12. Glass, W. G., K. Subbarao, B. Murphy, and P. M. Murphy. 2004. Mechanisms of host defense following severe acute respiratory syndrome-coronavirus (SARS-CoV) pulmonary infection of mice. *J. Immunol.* 173: 4030–4039.
13. Roberts, A., L. Vogel, J. Guarner, N. Hayes, B. Murphy, S. Zaki, and K. Subbarao. 2005. Severe acute respiratory syndrome coronavirus infection of golden Syrian hamsters. *J. Virol.* 79: 503–511.
14. ter Meulen, J., A. B. Bakker, E. N. van den Brink, G. J. Weverling, B. E. Martina, B. L. Haagmans, T. Kuiken, J. de Kruif, W. Preiser, W. Spaan, et al. 2004. Human monoclonal antibody as prophylaxis for SARS coronavirus infection in ferrets. *Lancet* 363: 2139–2141.
15. Roberts, A., C. Paddock, L. Vogel, E. Butler, S. Zaki, and K. Subbarao. 2005. Aged BALB/c mice as a model for increased severity of severe acute respiratory syndrome in elderly humans. *J. Virol.* 79: 5833–5838.
16. Hong, T. C., Q. L. Mai, D. V. Cuong, M. Parida, H. Minekawa, T. Notomi, F. Hasebe, and K. Morita. 2004. Development and evaluation of a novel loop-mediated isothermal amplification method for rapid detection of severe acute respiratory syndrome coronavirus. *J. Clin. Microbiol.* 42: 1956–1961.
17. Kitabatake, M., S. Inoue, F. Yasui, S. Yokochi, M. Arai, K. Morita, H. Shida, M. Kidokoro, F. Murai, M. Q. Le, K. Mizuno, et al. 2007. SARS-CoV spike protein-expressing recombinant vaccinia virus efficiently induces neutralizing antibodies in rabbits pre-immunized with vaccinia virus. *Vaccine* 25: 630–637.
18. Hsieh, P. K., S. C. Chang, C. C. Huang, T. T. Lee, C. W. Hsiao, Y. H. Kou, I. Y. Chen, C. K. Chang, T. H. Huang, and M. F. Chang. 2005. Assembly of severe acute respiratory syndrome coronavirus RNA packaging signal into virus-like particles is nucleocapsid dependent. *J. Virol.* 79: 13848–13855.
19. Zhang, C. H., J. H. Lu, Y. F. Wang, H. Y. Zheng, S. Xiong, M. Y. Zhang, X. J. Liu, J. X. Li, Z. Y. Wan, X. G. Yan, et al. 2005. Immune responses in BALB/c mice induced by a candidate SARS-CoV inactivated vaccine prepared from F69 strain. *Vaccine* 23: 3196–3201.
20. Biacchesi, S., M. H. Skiadopoulos, L. Yang, B. R. Murphy, P. L. Collins, and U. J. Buchholz. 2005. Rapid human metapneumovirus microneutralization assay based on green fluorescent protein expression. *J. Virol. Methods* 128: 192–197.
21. Cimolai, N., G. P. Taylor, D. Mah, and B. J. Morrison. 1992. Definition and application of a histopathological scoring scheme for an animal model of acute *Mycoplasma pneumoniae* pulmonary infection. *Microbiol. Immunol.* 36: 465–478.
22. Luna, L. G., 1968. *Manual of Histologic Staining Methods of the Armed Forces Institute of Pathology*. McGraw-Hill, New York, p. 111.
23. Voss, D., A. Kern, E. Traggiai, M. Eickmann, K. Stadler, A. Lanzavecchia, and S. Becker. 2006. Characterization of severe acute respiratory syndrome coronavirus membrane protein. *FEBS Lett.* 580: 968–973.
24. Ho, Y., P. H. Lin, C. Y. Liu, S. P. Lee, and Y. C. Chao. 2004. Assembly of human severe acute respiratory syndrome coronavirus-like particles. *Biochem. Biophys. Res. Commun.* 318: 833–838.
25. Huang, Y., Z. Y. Yang, W. P. Kong, and G. J. Nabel. 2004. Generation of synthetic severe acute respiratory syndrome coronavirus pseudoparticles: implications for assembly and vaccine production. *J. Virol.* 78: 12557–12565.
26. Buchholz, U. J., A. Bukreyev, L. Yang, E. W. Lamirande, B. R. Murphy, K. Subbarao, and P. L. Collins. 2004. Contributions of the structural proteins of severe acute respiratory syndrome coronavirus to protective immunity. *Proc. Natl. Acad. Sci. USA* 101: 9804–9809.
27. Kim, T. W., J. H. Lee, C. F. Hung, S. Peng, R. Roden, M. C. Wang, R. Viscidi, Y. C. Tsai, L. He, P. J. Chen, et al. 2004. Generation and characterization of DNA vaccines targeting the nucleocapsid protein of severe acute respiratory syndrome coronavirus. *J. Virol.* 78: 4638–4645.
28. Fan, B. X., L. X. Xie, L. A. Chen, W. J. Chen, J. Wen, and Y. N. Liu. 2005. Study on the dynamics of IgG antibody in 311 patients with severe acute respiratory syndrome. *Zhonghua Liu Xing Bing Xue Za Zhi.* 26: 194–196.
29. Che, X. Y., L. W. Qiu, Z. Y. Liao, Y. D. Wang, K. Wen, Y. X. Pan, W. Hao, Y. B. Mei, V. C. Cheng, and K. Y. Yuen. 2005. Antigenic cross-reactivity between severe acute respiratory syndrome-associated coronavirus and human coronaviruses 229E and OC43. *J. Infect. Dis.* 191: 2033–2037.
30. Cheng, M., C. W. Chan, R. C. Cheung, R. K. Bikkavilli, Q. Zhao, S. W. Au, P. K. Chan, S. S. Lee, G. Cheng, W. K. Ho, and W. T. Cheung. 2005. Cross-reactivity of antibody against SARS-coronavirus nucleocapsid protein with IL-11. *Biochem. Biophys. Res. Commun.* 338: 1654–1660.
31. Liu, S. J., C. H. Leng, S. P. Lien, H. Y. Chi, C. Y. Huang, C. L. Lin, W. C. Lian, C. J. Chen, S. L. Hsieh, and P. Chong. 2006. Immunological characterizations of the nucleocapsid protein based SARS vaccine candidates. *Vaccine* 24: 3100–3108.
32. Zhu, M. S., Y. Pan, H. Q. Chen, Y. Shen, X. C. Wang, Y. J. Sun, and K. H. Tao. 2004. Induction of SARS-nucleoprotein-specific immune response by use of DNA vaccine. *Immunol. Lett.* 92: 237–243.
33. Zhao, J., Q. Huang, W. Wang, Y. Zhang, P. Lv, and X. M. Gao. 2007. Identification and characterization of dominant helper T-cell epitopes in the nucleocapsid protein of severe acute respiratory syndrome coronavirus. *J. Virol.* 81: 6079–6088.
34. Yang, Z. Y., W. P. Kong, Y. Huang, A. Roberts, B. R. Murphy, K. Subbarao, and G. J. Nabel. 2004. A DNA vaccine induces SARS coronavirus neutralization and protective immunity in mice. *Nature* 428: 561–564.
35. Bukreyev, A., E. W. Lamirande, U. J. Buchholz, L. N. Vogel, W. R. Elkins, M. St Claire, B. R. Murphy, K. Subbarao, and P. L. Collins. 2004. Mucosal immunisation of African green monkeys (*Cercopithecus aethiops*) with an attenuated parainfluenza virus expressing the SARS coronavirus spike protein for the prevention of SARS. *Lancet* 363: 2122–2127.
36. Zhi, Y., J. Figueredo, G. P. Kobinger, H. Hagan, R. Calcedo, J. R. Miller, G. Gao, and J. M. Wilson. 2006. Efficacy of severe acute respiratory syndrome vaccine based on a nonhuman primate adenovirus in the presence of immunity against human adenovirus. *Hum. Gene Ther.* 17: 500–506.
37. Bisht, H., A. Roberts, L. Vogel, K. Subbarao, and B. Moss. 2005. Neutralizing antibody and protective immunity to SARS coronavirus infection of mice induced by a soluble recombinant polypeptide containing an N-terminal segment of the spike glycoprotein. *Virology* 334: 160–165.
38. Bisht, H., A. Roberts, L. Vogel, A. Bukreyev, P. L. Collins, B. R. Murphy, K. Subbarao, and B. Moss. 2004. Severe acute respiratory syndrome coronavirus

spike protein expressed by attenuated vaccinia virus protectively immunizes mice. *Proc. Natl. Acad. Sci. USA* 101: 6641–6646.
39. Kapadia, S. U., J. K. Rose, E. Lamirande, L. Vogel, K. Subbarao, and A. Roberts. 2005. Long-term protection from SARS coronavirus infection conferred by a single immunization with an attenuated VSV-based vaccine. *Virology* 340: 174–182.
40. Jiang, Y., J. Xu, C. Zhou, Z. Wu, S. Zhong, J. Liu, W. Luo, T. Chen, Q. Qin, and P. Deng. 2005. Characterization of cytokine/chemokine profiles of severe acute respiratory syndrome. *Am. J. Respir. Crit. Care Med.* 171: 850–857.
41. Franks, T. J., P. Y. Chong, P. Chui, J. R. Galvin, R. M. Lourens, A. H. Reid, E. Selbs, C. P. McEvoy, C. D. Hayden, J. Fukuoka, et al. 2003. Lung pathology of severe acute respiratory syndrome (SARS): a study of 8 autopsy cases from Singapore. *Hum. Pathol.* 34: 743–748.
42. Nicholls, J. M., L. L. Poon, K. C. Lee, W. F. Ng, S. T. Lai, C. Y. Leung, C. M. Chu, P. K. Hui, K. L. Mak, W. Lim, et al. 2003. Lung pathology of fatal severe acute respiratory syndrome. *Lancet* 361: 1773–1778.
43. Ding, Y., H. Wang, H. Shen, Z. Li, J. Geng, H. Han, J. Cai, X. Li, W. Kang, D. Weng, et al. 2003. The clinical pathology of severe acute respiratory syndrome (SARS): a report from China. *J. Pathol.* 200: 282–289.
44. He, L., Y. Ding, Q. Zhang, X. Che, Y. He, H. Shen, H. Wang, Z. Li, L. Zhao, J. Geng, et al. 2006. Expression of elevated levels of pro-inflammatory cytokines in SARS-CoV-infected ACE2+ cells in SARS patients: relation to the acute lung injury and pathogenesis of SARS. *J. Pathol.* 210: 288–297.
45. Zhang, X., K. Wu, D. Wang, X. Yue, D. Song, Y. Zhu, and J. Wu. 2007. Nucleocapsid protein of SARS-CoV activates interleukin-6 expression through cellular transcription factor NF-κB. *Virology* 365: 324–335.
46. Fuss, I. J., M. Boirivant, B. Lacy, and W. Strober. 2002. The interrelated roles of TGF-β and IL-10 in the regulation of experimental colitis. *J. Immunol.* 168: 900–908.
47. Weingartl, H., M. Czub, S. Czub, J. Neufeld, P. Marszal, J. Gren, G. Smith, S. Jones, R. Proulx, Y. Deschambault, et al. 2004. Immunization with modified vaccinia virus Ankara-based recombinant vaccine against severe acute respiratory syndrome is associated with enhanced hepatitis in ferrets. *J. Virol.* 78: 12672–12676.
48. Czub, M., H. Weingartl, S. Czub, R. He, and J. Cao. 2005. Evaluation of modified vaccinia virus Ankara based recombinant SARS vaccine in ferrets. *Vaccine* 23: 2273–2279.
49. Corapi, W. V., C. W. Olsen, and F. W. Scott. 1992. Monoclonal antibody analysis of neutralization and antibody-dependent enhancement of feline infectious peritonitis virus. *J. Virol.* 66: 6695–6705.
50. Halstead, S. B. 1982. Immune enhancement of viral infection. *Prog. Allergy* 31: 301–364.
51. Deming, D., T. Sheahan, M. Heise, B. Yount, N. Davis, A. Sims, M. Suthar, J. Harkema, A. Whitmore, R. Pickles, et al. 2006. Vaccine efficacy in senescent mice challenged with recombinant SARS-CoV bearing epidemic and zoonotic spike variants. *PLoS Med.* 3:e525.
52. Boelen, A., A. Andeweg, J. Kwakkel, W. Lokhorst, T. Bestebroer, J. Dormans, and T. Kimman. 2000. Both immunisation with a formalin-inactivated respiratory syncytial virus (RSV) vaccine and a mock antigen vaccine induce severe lung pathology and a Th2 cytokine profile in RSV-challenged mice. *Vaccine* 19: 982–991.
53. Johnson, T. R., J. E. Johnson, S. R. Roberts, G. W. Wertz, R. A. Parker, and B. S. Graham. 1998. Priming with secreted glycoprotein G of respiratory syncytial virus (RSV) augments interleukin-5 production and tissue eosinophilia after RSV challenge. *J. Virol.* 72: 2871–2880.
54. Jin, H., C. Xiao, Z. Chen, Y. Kang, Y. Ma, K. Zhu, Q. Xie, Y. Tu, Y. Yu, and B. Wang. 2005. Induction of Th1 type response by DNA vaccinations with N, M, and E genes against SARS-CoV in mice. *Biochem. Bbiophys. Res. Commun.* 328: 979–986.
55. Shi, S. Q., J. P. Peng, Y. C. Li, C. Qin, G. D. Liang, L. Xu, Y. Yang, J. L. Wang, and Q. H. Sun. 2006. The expression of membrane protein augments the specific responses induced by SARS-CoV nucleocapsid DNA immunization. *Mol. Immunol.* 43: 1791–1798.
56. Faber, M., E. W. Lamirande, A. Roberts, A. B. Rice, H. Koprowski, B. Dietzschold, and M. J. Schnell. 2005. A single immunization with a rhabdovirus-based vector expressing severe acute respiratory syndrome coronavirus (SARS-CoV) S protein results in the production of high levels of SARS-CoV-neutralizing antibodies. *J. Gen. Virol.* 86: 1435–1440.
57. Du, L., G. Zhao, Y. Lin, H. Sui, C. Chan, S. Ma, Y. He, S. Jiang, C. Wu, K. Y. Yuen, et al. 2008. Intranasal vaccination of recombinant adeno-associated virus encoding receptor-binding domain of severe acute respiratory syndrome coronavirus (SARS-CoV) spike protein induces strong mucosal immune responses and provides long-term protection against SARS-CoV infection. *J. Immunol.* 180: 948–956.

Journal of Heredity 2008:99(3):254–264
doi:10.1093/jhered/esn003
Advance Access publication March 11, 2008

Mitochondrial DNA Sequence Phylogeny of 4 Populations of the Widely Distributed Cynomolgus Macaque (*Macaca fascicularis fascicularis*)

ANTOINE BLANCHER, MAXIME BONHOMME, BRIGITTE CROUAU-ROY, KEIJI TERAO, TAKASHI KITANO, AND NARUYA SAITOU

From the Laboratoire d'immunogénétique moléculaire, Université Paul Sabatier, Toulouse, France (Blancher); the Laboratoire d'immunologie, Hôpital Rangueil, TSA 50032, 31059 Toulouse cedex 9, France (Blancher); the Laboratoire UMR CNRS 5174 Evolution et Diversité Biologique, Université Paul Sabatier, Toulouse, France (Bonhomme and Crouau-Roy); the Primate Centre, National Institute of Infectious Diseases, 1-Hachimandai, Tsukuba, Ibaraki, 305-0843, Japan (Terao); and the Division of Population Genetics, National Institute of Genetics, Mishima, 411-8540, Japan (Kitano and Saitou). Takashi Kitano is now at the Faculty of Engineering, Ibaraki University, Hitachi, Japan.

Address correspondence to A. Blancher at the address above, or e-mail: blancher@easynet.fr.

Abstract

We studied the mitochondrial DNA (mtDNA) polymorphism of 304 *Macaca fascicularis fascicularis* (*M. f. fascicularis*) individuals, representative of 4 cynomolgus macaque populations (Indochina, Indonesia, Philippines, and Mauritius). By sequencing a 590-bp fragment in the hypervariable II region of the D-loop region, we defined 70 haplotypes. The homologous region was also characterized in 22 Chinese *Macaca mulatta* and 2 *Macaca sylvanus*. The phylogenetic analysis confirms the monophyly of *M. f. fascicularis* and defines 2 haplotype groups inside the *M. f. fascicularis* clade: one "insular," encompassing 6 Philippines, 2 Mauritius, and 31 Indonesian haplotypes, the other "continental" that contains all Indochinese and 6 Indonesian haplotypes. Continental and insular group divergence time was estimated to be approximately 10^6 years before present (BP). Among Indonesian haplotypes, some have a continental origin. This suggests either direct migration from mainland to Indonesia or that remnant lineages from an ancient population genetically close to the mainland (i.e., in the Sunda Shelf, <550 000 years BP) were subsequently brought southward to Indonesia. The low nucleotide diversity in the Philippines population suggests a bottleneck following colonization by Indonesian individuals, around 110 000 years BP. mtDNA and further observations of nuclear genetic data corroborate the mixed origin (Indonesian/continental) hypothesis of Mauritius individuals and a population bottleneck.

Cynomolgus macaque (*Macaca fascicularis*) is used as a non-human primate model for biomedical research in various domains such as tissue allograft rejection in case of kidney (Boric et al. 2002; Wieczorek et al. 2006) or cardiac (Schroder et al. 2007) transplantation, bone marrow graft (Lau et al. 2004), immune response against pathogens (Sato et al. 2008) or new vaccines (Kita et al. 2005), and infectious diseases and particularly Simian Immunodeficiency Virus (SIV)-induced AIDS or emergent pathogens (Kuiken et al. 2003; Reed et al. 2005; Lawler et al. 2006). In all these models, the genetic background of the animals could be of great importance; in some cases, it was reported that animal geographical origin can influence the response to drugs or the sensibility to the experimental disease (Schmidt et al. 1977; Menninger et al. 2002). Numerous reports have been published on the geographical variations of the cynomolgus macaque. Blood groups (Terao et al. 1981), blood proteins (Nozawa et al. 1977; Kondo et al. 1993), mitochondrial DNA (mtDNA) (Harihara et al. 1988; Lawler et al. 1995; Tosi et al. 2002, 2003; Smith et al. 2007; Tosi and Coke 2007), and Y chromosome DNA (Tosi et al. 2002, 2003; Tosi and Coke 2007) were studied. The phylogenetic relationships among the populations of *M. fascicularis* have been discussed, and discrepancies in population divergence times between mtDNA and nuclear markers have been found. Moreover, the analysis of paleoclimate in South Asia has led some authors to propose various hypotheses concerning the geographical dispersal of macaques in

Southeast Asia (Fooden 1995; Delson 1980; Eudey 1980; Abegg and Thierry 2002). The cynomolgus macaque is characterized by its habitat, the mangroves (Fittinghoff and Lindburg 1980; Wheatley 1980), which may have favored a dispersal mode through the estuaries and by sea rafting. Thus, both habitat characteristics and past sea level changes in Southeast Asia could explain the wide geographic distribution of the species. This study focuses on the common subspecies *Macaca fascicularis fascicularis* (*M. f. fascicularis*), excluding all other subspecies that are either restricted to some small islands or morphologically different (i.e., the dark pelage subspecies *Macaca fascicularis philippinensis*), as extensively described in Fooden (1991, 1995).

Maternally inherited mtDNA has provided valuable data for investigating intraspecific variation, population structure, phylogeography, and demography in macaque species (Harihara et al. 1988; Melnick and Hoelzer 1992; Lawler et al. 1995; Tosi et al. 2002; Marmi et al. 2004; Modolo et al. 2005; Smith and McDonough 2005; Kawamoto, Shotake, et al. 2007; Smith et al. 2007). Harihara et al. (1988), through restriction fragment length polymorphism (RFLP) data on *M. fascicularis* populations using 5 restriction enzymes applied to 149 individuals, described 2 population groups: "insular" (Philippines and Indonesia) and "continental" (Malaysia and Indochina). The genetic distance between the haplotypes of these 2 groups suggests a deep split between the continental and the insular groups. The dichotomy between insular and continental populations was confirmed by Tosi et al. (2002, 2003) and Tosi and Coke (2007). However, the mtDNA lineage heterogeneity found for the Indonesian population suggests a complex origin.

Lawler et al. (1995) showed that cynomolgus macaque from Mauritius have only a few mitochondrial RFLP haplotypes, all possibly deriving from a single one. This observation indicates a recent founding of the Mauritius macaque population by an artificial introduction between 300 and 500 years ago (see Sussman and Tattersall 1986). Sailors imported a few animals most probably from Indonesia, as confirmed by the genetic proximity of 1) Mauritius and Java populations using nuclear and mtDNA markers (Kondo et al. 1993; Kawamoto Y, Kawamoto S, et al. 2008, Tosi and Coke 2007) and of 2) Mauritius and Sumatra by means of Y chromosome sequences (Tosi and Coke 2007).

In the present study, we investigate the molecular genetic relationships between cynomolgus macaque populations and one rhesus macaque (*Macaca mulatta*) population, using mtDNA sequence data. The aim of this study is to refine more precisely the phylogeographic structure of the cynomolgus macaque, to make inferences about the dispersal scenario of this species, and to confront mtDNA polymorphism to nuclear genetic diversity (Bonhomme et al. 2007) in the same samples. Herein, we sequenced around 590 bp in hypervariable segment 2 (HVII) of the D-loop of a large number of individuals (304) from 4 cynomolgus macaque populations (Indochina, Indonesia, Philippines, and Mauritius island). The artificially established Mauritius population was studied to trace the most probable ancestral population and the signature of the founding effect. The phylogenetic relationships of the 3 natural populations (Indonesia, Indochina, and Philippines) are discussed with regard to the colonization of Southeast Asia by *M. f. fascicularis*.

Materials and Methods

Animals and DNA Samples

Genomic DNA was extracted from peripheral blood of 304 unrelated *M. f. fascicularis* using either QIA amp Blood Kit (Qiagen, Courtaboeuf, France) or phenol-chloroform extraction. DNA blood samples of 137 animals captured from the Indonesian wild population were obtained from the Tsukuba Primate Center through K.T. Other animals are F_1 derived from breeders that had been captured in the wild on various locations in Mauritius ($N = 74$), Philippines ($N = 25$), and Indochina ($N = 68$) by Noveprim (Mauritius), Siconbrec (Philippines), and Nafovanny (Vietnam), respectively. *Macaca mulatta* blood samples ($N = 22$) were obtained from the Bioprim quarantine center (Bioprim, Baziège, France). The rhesus monkeys were F_1 imported from a Chinese breeding center (South China Primate Research Development Center, Jiufu center, Guangzhou, China). *Macaca sylvanus* blood samples from 2 unrelated individuals were provided by Dr. Ducos de Lahitte (Ecole Nationale Vétérinaire, Toulouse, France).

Polymerase Chain Reaction and Sequencing

A 590-bp fragment of the HVII of the mtDNA D-loop was amplified by using the pair of primers: Saru-4F (5′-ATCACGGGTCTATCACCCTA-3′) and Saru-5R (5′-GGCCAGGACCAAGCCTATTT-3′). This primer pair has been successfully used for Japanese macaque mtDNA studies (Hayasaka et al. 1991; Kawamoto, Shotake, et al. 2007) and is also known to produce no amplification of nuclear-inserted mtDNA sequences in *M. f. fascicularis* (Dr. Kawamoto Y, personal communication). This pair amplifies positions 22–606 in the complete sequence of *M. mulatta* mitochondrial genome (DNA Databank of Japan-DDBJ/European Molecular Biology Laboratory-EMBL/GenBank accession number AY612638).

Amplified material was separated on agarose gels, purified by using QIAquick PCR Purification Kit (Qiagen, Courtaboeuf, France), and directly sequenced on both strands by the fluorescent Dye Terminator method on an ABI 373 automatic sequencer (Applied Biosystems Japan, Tokyo, Japan) or an CEQ 2000 automatic sequencer (Beckman Coulter, Paris, France). In all population samples, we paid special attention to sequences differing from the most frequent and checked all these sequences by sequencing again the target fragment.

Sequence Data Analysis

The *M. f. fascicularis* sequences characterized were aligned with macaque mtDNA sequences obtained from 2 *M. sylvanus* and 22 *M. mulatta* (this study) and homologous sequences available in DDBJ/EMBL/GenBank International Nucleotide Sequence Database (2 *Macaca fuscata* and 1 *Papio hamadryas*, accession numbers M80209, M80210, and

Y18001). Nucleotide diversity π (Nei 1987), Tajima's D (Tajima 1989), and Fu's (1997) F_s were calculated using the ARLEQUIN ver. 2.000 package (Schneider et al. 2000) on the HVII region dataset reported here and on the HVI region dataset of Smith et al. (2007). We constructed phylogenetic trees, based on 590 nucleotides, using 3 different methods. First, a neighbor-joining tree (Saitou and Nei 1987) was constructed with the Kimura's 2-parameter distance (Kimura 1980), using the computer program MEGA ver. 3.0 (Kumar et al. 2004), and 10 000 bootstraps were performed to determine the significance of tree branching. We then performed maximum likelihood (ML) and Bayesian phylogenetic analyses using the most likely substitution model inferred using a likelihood framework implemented in the software MODELTEST 3.7 (Posada and Crendall 1998). This software tests 56 different substitution models and estimates the most likely one using a likelihood ratio test. ML inference was performed using the PHYML software (Guindon and Gascuel 2003), and 10 000 bootstraps were performed on the ML tree. Finally, a Bayesian analysis was performed using the software MrBayes (Ronquist and Huelsenbeck 2003), where 2 Markov Chains were run on 10×10^6 generations with a sampling each 100 generations. Such a run length allowed the standard deviation of allelic frequencies to pass below 0.01 and the potential scale reduction factor to reach a value of 1, as suggested by the authors. The first 25 000 trees (25%) were discarded from the analysis as a burn-in.

Results

Determination of mtDNA Sequences

Primate mtDNA is known to be often inserted into nuclear DNA—"numts"—(Bensasson et al. 2001). Numts were shown to hinder the evolutionary history inference of primate species (Thalmann et al. 2004, 2005). Thus, we carefully considered the putative amplification and sequencing of numts, although caution was done when choosing the polymerase chain reaction (PCR) primers (see Materials and Methods). With all *M. fascicularis* samples, we obtained a single band by PCR amplification, and most direct sequencing results showed unique nucleotide sequence for each individual. As for *M. mulatta* samples, about 1/3 of PCR products did not show unique sequence, so we chose ones that were very close to the complete sequence of *M. mulatta* mitochondrial genome (DDBJ/EMBL/GenBank accession number AY612638). Our 2 newly determined *M. sylvanus* sequences were also compared with the complete sequence of *M. sylvanus* mitochondrial genome (DDBJ/EMBL/GenBank accession number AJ309865), and they were found to be very close with each other. Furthermore, phylogenetic analyses of these sequences produced trees consistent with the known macaque phylogeny (see below). In conclusion, we believe that our nucleotide sequences were derived from authentic mtDNA. Nucleotide sequences determined in this study were deposited to the DDBJ/EMBL/GenBank under accession numbers AB261898–AB261974.

Macaca fascicularis fascicularis mtDNA Sequence Diversity

In total, 120 positions are polymorphic in 304 individuals, including 8 positions with indels (Figure 1), for a total of 70 haplotypes. Among the 112 positions with substitutions, 109 are dimorphic with transitions being much more frequent (65 C $\leftrightarrow$ T and 38 A $\leftrightarrow$ G) than transversions (6 in total). Only 2 populations, Indonesia and Mauritius, share one haplotype that is present in all Mauritius animals but one and in 6 out of 137 animals from Indonesia.

The intrapopulation diversity is shown in Table 1(a). Nucleotide diversity (π) was the highest (0.032) for Indonesia, followed by Indochina (0.017) and Philippines population (0.009). The Mauritius population has only 2 haplotypes differing by a single-base substitution. Accordingly, the nucleotide diversity (4.6×10^{-5}) was extremely low for this population. The gene diversity (h) in Indochina and Indonesia is similar in our study (HVII) and in that of Smith et al. (2007) based on HVI, as shown in Table 1 (a, b). However, gene diversity is higher with HVI than with HVII in Philippines and Mauritius. The nucleotide diversity is at least 5 times higher for HVI than for HVII in all populations. This confirms, in *M. f. fascicularis*, the higher mutation rate in the HVI region than in the HVII region of the D-loop, found in humans (Meyer et al. 1999). Except for Mauritius, both neutrality tests for HVI and HVII reveal that polymorphism is neutral, as expected for the mtDNA D-loop region. In the case of the Mauritius population, only HVI (and not HVII) analysis revealed significantly negative F_S and D values. The greater polymorphism of HVI may thus indicate a recent expansion in the Mauritius population.

Phylogenetic Analysis

The neighbor-joining, ML, and Bayesian trees have the same topology. We thus show only the Bayesian tree (Figure 2). All the *M. f. fascicularis* sequences clustered together (posterior value = 91%), showing that *M. f. fascicularis* is monophyletic.

Inside the *M. f. fascicularis* clade, 2 main groups of sequences can be detected. Group I encompasses all haplotypes from the Philippines and Mauritius samples and most of the Indonesian sample haplotypes (29 out of 35). The sequences from the Philippines population and that from one Indonesian individual constitute a subgroup I-1 (posterior value = 85%). There are 3 other subclusters in group I (I-2, I-3, and I-4), all supported with posterior values higher than 77% (see Figure 2). Two Mauritius haplotypes belong to subcluster I-3 with 14 Indonesian haplotypes (posterior value = 98%), and the remaining 3 subclusters (I-2 and I-4) consist of 2 and 12 Indonesian haplotypes, respectively. Group II includes all Indochinese haplotypes and 6 haplotypes from Indonesia, and we divided it into 3 subclusters (II-1, II-2, and II-3), as shown in Figure 2. Subclusters II-1 and II-3 include haplotypes only found in Indochina (2 and 25, respectively), whereas subcluster II-2 consists of 6 Indonesian haplotypes that are closer to Indochinese haplotypes than to Indonesian haplotypes of group I (posterior value = 97%).